# ATF4 Regulates MYB to Increase γ-Globin in Response to Loss of β-Globin

## Graphical Abstract



Modeling erythroid stress upon reduction of β-globin

## Authors

Mandy Y. Boontanrart,
Markus S. Schröder, Gautier M. Stehli, ...,
Benjamin G. Gowen, Mark A. DeWitt,
Jacob E. Corn

## Correspondence

jacob.corn@biol.ethz.ch

## In Brief

Boontanrart et al. model the cellular stress that occurs upon loss of β-globin in human erythroid cells. Decreased β-globin attenuates the eIF2aP-ATF4 pathway, resulting in increased fetal γ-globin. ATF4 regulates the MYB γ-globin repressor via binding at the *HBS1L-MYB* intergenic enhancer.

## Highlights

- Loss of β-globin leads to upregulation of γ-globin via altered ATF4 signaling

- Reduced ATF4 decreases the levels of MYB and BCL11A

- ATF4 induces MYB through binding at the *HBS1L-MYB* intergenic enhancer

CellPress

# Cell Reports

## Article

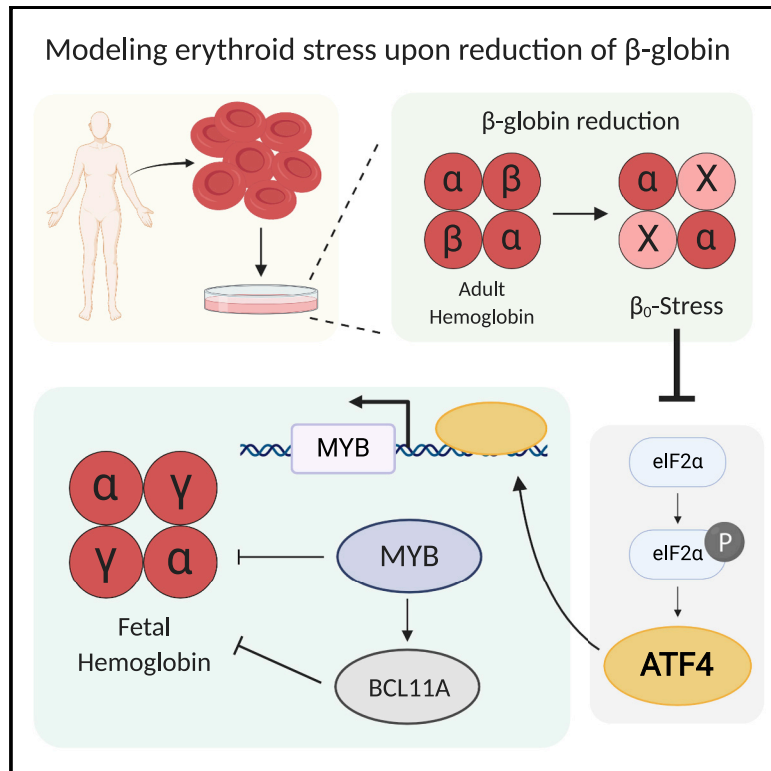# ATF4 Regulates MYB to Increase γ-Globin in Response to Loss of β-Globin

Mandy Y. Boontanrart,[1] Markus S. Schröder,[2] Gautier M. Stehli,[2] Marija Banović,[2] Stacia K. Wyman,[1,3] Rachel J. Lew,[1] Matteo Bordi,[2] Benjamin G. Gowen,[1,4] Mark A. DeWitt,[1] and Jacob E. Corn[1,2,3,5,*]
[1]Department of Molecular and Cell Biology, University of California, Berkeley, Berkeley, CA 94720, USA
[2]Department of Biology, ETH Zurich, Zurich 8092, Switzerland
[3]Innovative Genomics Institute, University of California, Berkeley, Berkeley, CA 94720, USA
[4]Present address: Spotlight Therapeutics, Hayward, CA 94545, USA
[5]Lead Contact
*Correspondence: jacob.corn@biol.ethz.ch
https://doi.org/10.1016/j.celrep.2020.107993

## SUMMARY

β-Hemoglobinopathies can trigger rapid production of red blood cells in a process known as stress erythropoiesis. Cellular stress prompts differentiating erythroid precursors to express high levels of fetal γ-globin. However, the mechanisms underlying γ-globin production during cellular stress are still poorly defined. Here, we use CRISPR-Cas genome editing to model the stress caused by reduced levels of adult β-globin. We find that decreased β-globin is sufficient to induce robust re-expression of γ-globin, and RNA sequencing (RNA-seq) of differentiating isogenic erythroid precursors implicates ATF4 as a causal regulator of this response. ATF4 binds within the *HBS1L-MYB* intergenic enhancer and regulates expression of MYB, a known γ-globin regulator. Overall, the reduction of ATF4 upon β-globin knockout decreases the levels of *MYB* and *BCL11A*. Identification of ATF4 as a key regulator of globin compensation adds mechanistic insight to the poorly understood phenomenon of stress-induced globin compensation and could inform strategies to treat hemoglobinopathies.

## INTRODUCTION

Red blood cells (RBCs), also known as erythrocytes, are packed with hemoglobin tetramers and circulate throughout the body to supply all tissues with oxygen. Adult RBCs primarily contain adult hemoglobin (HbA), which consists of two copies of α-globin and two copies of β-globin. β-Thalassemic genetic disorders are caused by disruption of β-globin expression, causing loss of HbA and resulting in severe anemia, poor growth, and dramatically shortened lifespan. β-Thalassemia can be ameliorated by re-expression of γ-globin, which complexes with α-globin to form fetal hemoglobin (HbF). γ-Globin is normally expressed during development and silenced soon after birth, in an inverse relationship with β-globin.

Severe anemias such as β-thalassemia can trigger rapid production of RBCs in a process known as stress erythropoiesis. Stress erythropoiesis is induced by tissue hypoxia resulting from anemia and involves a distinct erythropoietic program that favors increased γ-globin. For example, recovery from bone marrow transplant or other treatments that greatly reduce erythroblast levels is often characterized by high levels of γ-globin and HbF (Alter, 1979; Meletis et al., 1994; Papayanno-poulou et al., 1980; Weinberg et al., 1986). Homozygous β-thalassemia patients transplanted with bone marrow from heterozygous siblings express high levels of HbF that can be sustained for up to 2 years after transplant (Galanello et al.,

1989). β-Thalassemia patients can also re-express high levels of γ-globin without transplant (Manca and Masala, 2008; Rochette et al., 1994). Intrinsic cellular processes can also mimic stress erythropoiesis, and *ex-vivo*-cultured stress erythroid progenitors express high levels of HbF (Xiang et al., 2015). Overall, this has led to the suggestion that erythroid stress recapitulates fetal erythropoiesis, but the pathways involved in fetal globin expression during this process remain to be determined.

HbF reactivation is being actively explored as a potential route to treat a variety of globinopathies, including β-thalassemia and sickle cell disease (Platt et al., 1984; Wienert et al., 2018). These approaches stem from the observation that naturally occurring mutations that promote HbF re-expression can ameliorate β-globinopathy symptoms (Berry et al., 1992; Jacob and Raper, 1958). A variety of strategies for HbF re-expression are being pursued, including large deletions within the β-globin locus, mutations of the *HBG*1/2 promoter, and cell-specific reduction of the BCL11A repressor by enhancer editing (Sankaran, 2011; Wienert et al., 2018).

Here, we sought to model the cellular erythroid stress occurring after disruption of β-globin, hereafter referred to as $\beta_0$-stress, in order to determine the mechanism underlying spontaneous re-expression of fetal hemoglobin. We and others previously found that HbF was upregulated after genome editing of *HBB* in CD34^{+} adult mobilized hematopoietic stem and progenitor cells (HSPCs) to reverse the causative allele of sickle cell

disease. *In vitro* differentiation of bulk-edited cell populations induced high *HBG*1/2 transcript levels as compared to unedited cells, which translated to high levels of HbF tetramers (DeWitt et al., 2016; Park et al., 2019; Vakulskas et al., 2018). This effect persisted even after long-term xenotransplantation of edited cells to immunodeficient mice (Magis et al., 2019).

We now show that $\beta_0$-stress caused by reductions in $\beta$-globin using either CRISPR-Cas genome editing or CRISPR interference (CRISPRi) transcriptional repression are sufficient to induce increased levels of $\gamma$-globin in immortalized hematopoietic progenitors and adult mobilized CD34^{+} HSPCs. Time-course transcriptomics of isogenic *HBB* knockout and wild-type (WT) cells during erythroid differentiation reveals that loss of $\beta$-globin leads to a transcriptional program that induces very high levels of *HBG* and moderately activates the transcription of other globins such as *HBE* and *HBZ*. Pathway analysis indicates that $\beta$-globin knockout cells reduce ATF4 (activating transcription factor 4) activity, leading to reductions in transcripts of many ATF4 targets. Endogenous mutation of ATF4 leads to upregulation of several globins, especially $\gamma$-globin, much like *HBB* knockout or knockdown. BCL11A levels were reduced in cells with knockout of *HBB* or an *ATF4* mutation, leading us to first suspect BCL11A as a possible ATF4 target. However, chromatin immunoprecipitation sequencing (ChIP-seq) showed no evidence for ATF4 binding anywhere near *BCL11A* regardless of differentiation status or *HBB* genotype. Instead, we find evidence for ATF4 binding within the *HBS1L-MYB* intergenic enhancer region. *MYB is* a known regulator of HbF expression at multiple levels, including promotion of *BCL11A* expression. (Antoniani et al., 2017). *MYB* transcript levels were reduced in cells with *HBB* knockout or harboring an *ATF4* mutation. Lastly, we found that *HBB* knockout reduces ATF4 binding at multiple genes involved in the unfolded protein response, leading to their transcriptional repression. Overall, our data indicate that $\beta_0$-stress inhibits an ATF4-mediated transcriptional program, which paradoxically reduces the unfolded protein response despite the presence of free $\alpha$-globin. Reduced ATF4 lowers *MYB* and BCL11A expression to upregulate multiple globins, especially $\gamma$-globin. These data provide mechanistic insight into the long-observed but poorly understood phenomenon of fetal globin expression during cell-intrinsic erythroid stress.

## RESULTS

### Loss of *HBB* Leads to Upregulation of $\gamma$-Globin

We previously observed that CRISPR-Cas9 editing at *HBB* in CD34^{+} mobilized peripheral blood HSPCs induced $\gamma$-globin transcription relative to unedited cells, leading to the formation of HbF tetramers (DeWitt et al., 2016). To mechanistically investigate how $\beta_0$-stress caused by knockout of *HBB* upregulates *HBG*, we used the HUDEP-2 cord-blood-derived erythroid progenitor cell line (Kurita et al., 2013). HUDEP-2 cells normally express high levels of *HBB* and low levels of *HBG*, making them a popular model for the study of adult globin regulation (Bauer et al., 2013; Grevet et al., 2018; Wienert et al., 2017).

We made a clonal HUDEP-2 line with homozygous knockout of *HBB* (HBBko) using electroporation of a CRISPR-Cas9 ribonucleoprotein (RNP) complexed with a well-validated *HBB*-target-

ing guide "e66," which targets the exonic (e) region 66 bp from the start of *HBB* (DeWitt et al., 2016) (Figure S1A). HBBko was derived from a WT HUDEP-2 clone (previously published as H2.1) in order to control for clonal effects associated with the heterogeneous HUDEP-2 parental population (Chung et al., 2019a; Wienert et al., 2017). $\gamma$-Globin levels were strikingly increased in the HBBko line by intracellular flow cytometry, with the vast majority of edited cells expressing detectable levels of the protein (Figure 1A).

Both the WT and HBBko lines were equally well *in vitro* differentiated to erythroblasts under standard conditions, as measured by staining for CD235a (glycophorin A). WT and HBBko cells exhibited no apparent difference in cell survival during bulk differentiation, suggesting that $\beta_0$-stress induces $\gamma$-globin expression in the majority of cells as opposed to conferring a fitness advantage toward cells that stochastically express more $\gamma$-globin (Figure S1B). WT expressed high levels of $\beta$-globin after differentiation, but as expected, HBBko completely lost $\beta$-globin protein by intracellular fluorescence-activated cell sorting (FACS). *HBB* mRNA was still detectable by qRT-PCR in HBBko but was slightly reduced relative to WT in undifferentiated cells and 95% reduced in differentiated cells (Figure S1C).

DNA damage associated with CRISPR-Cas9 genome editing has been linked to long-lasting cellular phenotypes in HSPCs, including p53 activation (Schiroli et al., 2019). To distinguish nonspecific effects of genome editing from specific intervention at the $\beta$-globin locus, we tested a panel of Cas9 RNPs complexed with *HBB* guide RNAs targeting exonic or neighboring intronic regions of *HBB* (Figure 1B). After bulk editing and *in vitro* differentiating the WT line, we found that multiple RNPs targeting coding regions consistently reduced *HBB* levels and increased *HBG*, as measured by qRT-PCR (Figures 1C and 1D). RNPs targeting neighboring intronic regions neither decreased *HBB* nor increased *HBG* despite similar levels of editing (Figure S1D). We found similar results when editing and *in vitro* differentiating CD34^{+} adult mobilized HSPCs from multiple donors with a panel of exonic or intronic *HBB*-targeting Cas9 RNPs (Figures S1E and S1F). Bulk editing *HBB* in CD34^{+} HSPC cells did not significantly alter cell numbers during expansion (Figure S1G). Additionally, total cell numbers after *in vitro* differentiation were comparable among exonic and intronic *HBB*-targeting guides (Figure S1H). As with isogenically edited HUDEP-2 cells, this implies that $\beta_0$-stress in HSPCs induces $\gamma$-globin expression rather than positively selecting for cells that already express $\gamma$-globin.

The ability of multiple *HBB*-targeting RNPs to induce *HBG* expression suggested that this effect was independent of the genomic change and was instead a response to loss of *HBB* transcript. To test this hypothesis, we made a stable WT HUDEP-2 subclone expressing dCas9-KRAB (CRISPRi) (Figure S1I). We found that stable CRISPRi of *HBB* using two different guide RNAs led to potent downregulation of $\beta$-globin and upregulation of $\gamma$-globin protein by intracellular flow cytometry (Figure 1E). This was also reflected by levels of *HBB* and *HBG* transcripts as measured by qRT-PCR (Figure S1J). Overall, these data indicate that upregulation of *HBG* is not a consequence of DNA damage or genomic targeting but is induced by loss of *HBB*.

To better characterize the globin protein composition resulting from loss of *HBB*, we used high-performance liquid
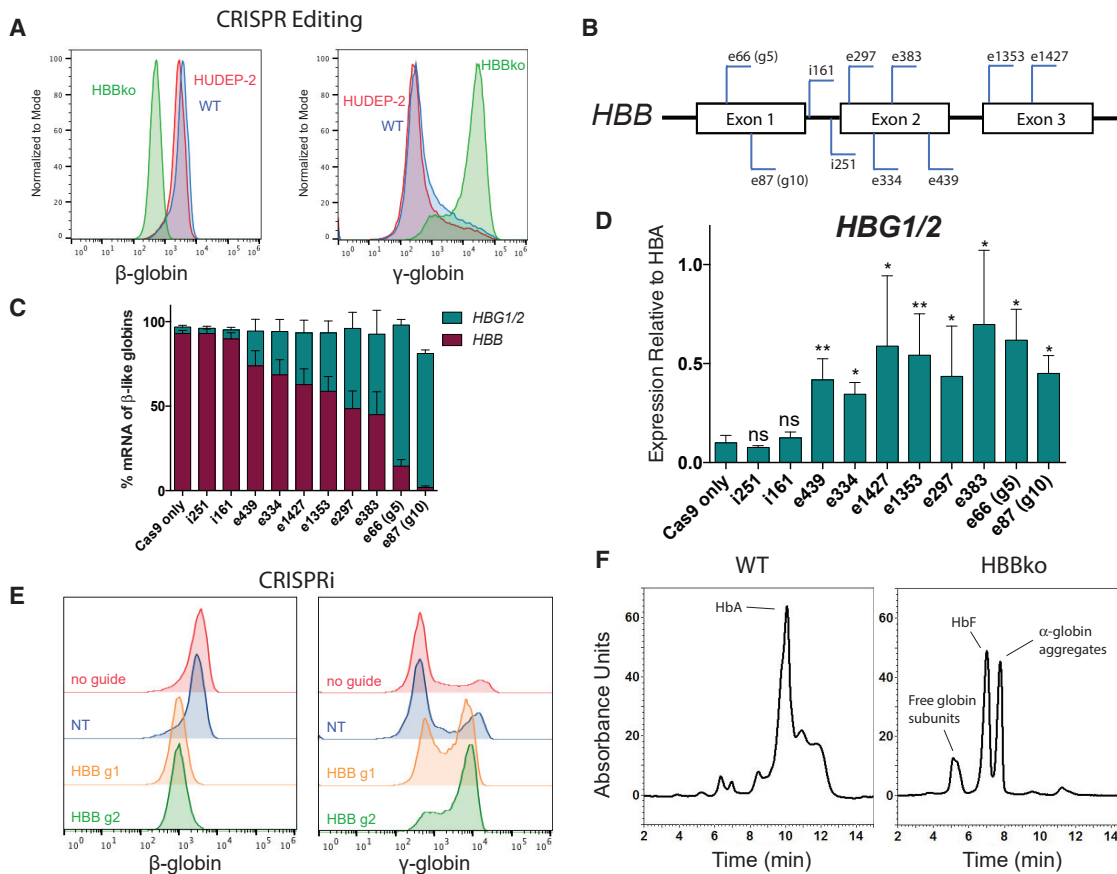
**Figure 1. Loss of β-Globin Leads to Increased γ-Globin in HUDEP-2 Cells and CD34⁺ HSPCs**

(A) A homozygous knockout of HBB (HBBko) was generated from a wild-type (WT) HUDEP-2 subclone though Cas9 ribonucleoprotein (RNP) targeting of exon 1 of *HBB*. Intracellular flow cytometry staining of β-globin and γ-globin of differentiated HUDEP-2 pool, WT clone, and HBBko clone.

(B) Schematic of single guide RNAs (sgRNAs) targeting *HBB* at either exonic (e) or intronic (i) positions. Numbers indicate the number of bases each RNP would cut after the transcription start site of the *HBB* gene. Previously published "G5" and "G10" sgRNAs are noted (DeWitt et al., 2016).

(C) qRT-PCR of *HBB* and *HBG1/2* after pooled editing of the WT line with each sgRNA and 5 days of differentiation. Data are plotted as percentage of all β-like globins (*HBE*, *HBB*, *HBG1/2*, and *HBD*) and presented as mean ± SD of three biological replicates.

(D) qRT-PCR of *HBB* and *HBG1/2* plotted relative to *HBA* transcripts. Editing efficiency of each sgRNA is shown in Figure S1D. The data are presented as mean ± SD of three biological replicates. p value indicates paired, two-tailed Student's t test (ns, nonsignificant; *p ≤ 0.05; **p ≤ 0.01).

(E) WT HUDEP-2 cells stably expressing dCas9-KRAB with guides targeting *HBB* were differentiated for 5 days, and hemoglobin levels were measured by intracellular flow cytometry.

(F) WT and HBBko cells were differentiated for 5 days, and hemolysates were analyzed by HPLC. Peak compositions were identified through mass spectrometry (Table S1).

chromatography (HPLC) coupled to mass spectrometry (MS) of *in vitro* differentiated HUDEP-2 clones. We separated intact globin peaks using standard HPLC conditions while also collecting fractions. We subjected each fraction to mass spectrometry in order to unambiguously assign the globin composition of each peak. HPLC of the WT clone resulted in a peak pattern suggesting a typically "adult" set of globins, including high levels of HbA (Figure 1F). This peak assignment was confirmed on the molecular level by mass spectrometry (Table S1). HPLC of the HBBko clone instead revealed a very different pattern of peaks (Figure 1F). Mass spectrometry and comparison to literature globin HPLC led us to assign these as uncomplexed globins, α-globin aggregates, and HbF tetramers (Lechauve et al., 2019) (Table S1).

Our data thus far indicate that low levels of *HBB* caused by either genome editing or CRISPRi are associated with high levels of *HBG*. The presence of α-globin aggregates in cells with β₀-stress suggests that an imbalance of hemoglobin proteins might lead to an unfolded protein response.

We therefore asked whether the relationship between levels of *HBB* and *HBG* was specific for reductions in *HBB* or a reflected an issue of general globin balance. For this, we utilized HUDEP-1 cells, which are similar to HUDEP-2 s but exhibit a mostly immature globin profile of low *HBB* and high *HBG*. Pooled knockout of *HBG* using a CRISPR-Cas RNP led to loss of *HBG* mRNA and upregulation of *HBB* (Figure S1K). Therefore, our data suggest that erythroid progenitors sense globin levels during differentiation and attempt to compensate for missing globins by
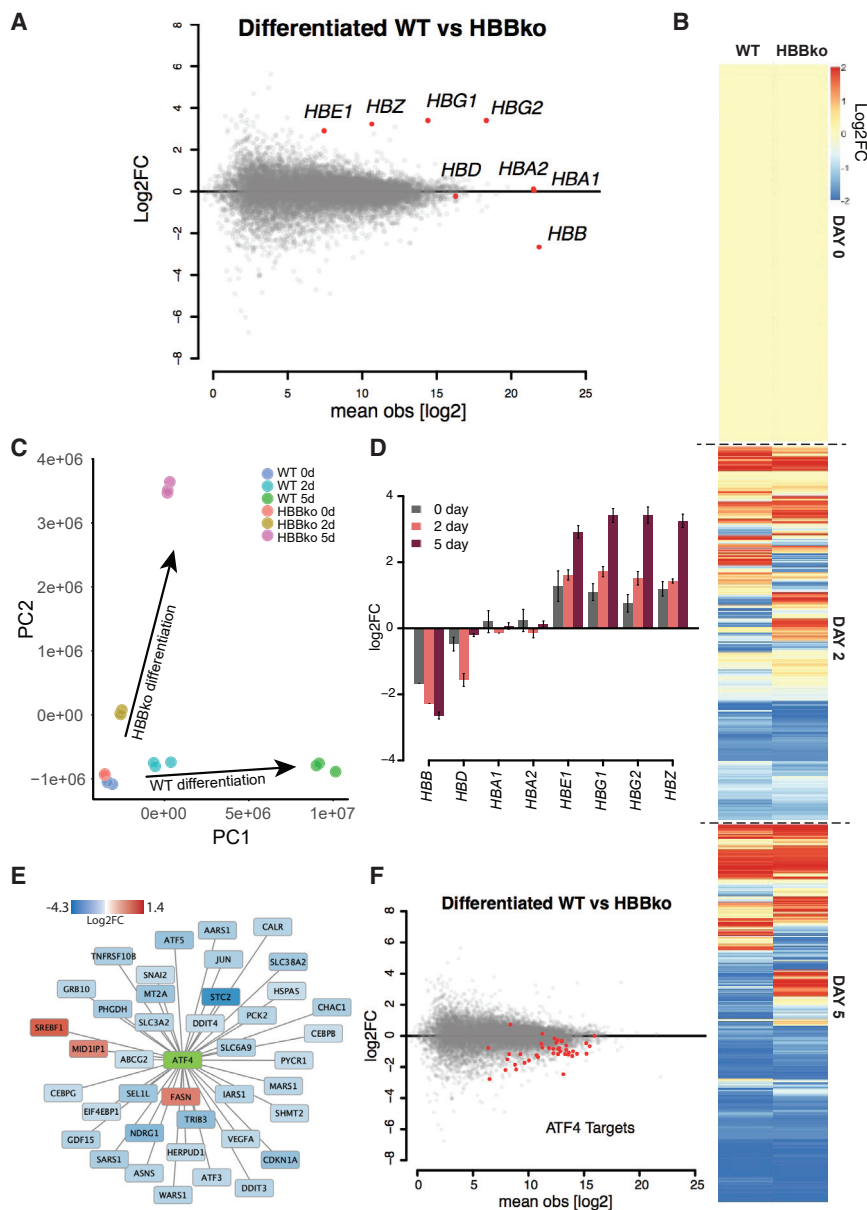
**Figure 2. Transcriptomics of Time-Course Differentiation Reveals an ATF4 Signature in HBBko Cells**

(A) MA plot after 5 days of differentiation comparing HBBko and WT cells. Globin genes are highlighted in red. RNA-seq was performed in biological triplicates, and data are shown as the mean.

(B) Biological triplicate RNA-seq data of WT and HBBko cells undifferentiated (day 0), after 2 days of differentiation, and after 5 days of differentiation. Transcript levels are expressed as log$_2$ fold change normalized to their respective day 0 expression.

(C) Principal-component analysis of all RNA-seq samples shows agreement of replicates and alterations in differentiation trajectories between WT and HBBko. Replicated colors indicate n = 3 biological replicates of each condition.

(D) The expression of embryonic, fetal, and adult globin genes is plotted for the three time points of differentiation. Data are shown as log2 fold change relative to WT cells and presented as mean ± SD of three biological replicates.

(E) Pathway analysis identifies 38 out of 40 ATF4 targets as significantly affected in HBBko cells. Genes highlighted in blue and red are ATF4 targets that are downregulated and upregulated genes by log2 fold change on day 5 of differentiation, respectively.

(F) MA plot from 5 days of differentiation highlighting 40 known ATF4 targets (red). The mean of biological triplicates is shown.

*HBG2*, *HBE*, and *HBZ* (Figure 2A). There were relatively low total levels of *HBE* and *HBZ* in HBBko cells after differentiation, such that *HBG1/2* comprised the vast majority of globin transcripts.

To capture the dynamics of differentiation, we performed triplicate time-course RNA-seq by collecting samples in their undifferentiated state, after 2 days of differentiation, and after 5 days of differentiation (Figures S2A and S2B). Globally, the transcriptomes of WT and *HBB* knockout cells are similar throughout differentiation (Figure S2C). However, on top of the overall similarity, the knockout of *HBB* induces a distinct transcriptional response that emerged after 2 days of differentiation and intensified by 5 days (Figure 2B). This was reflected in principal-component analysis (PCA), showing that WT and HBBko cells start quite similar but have distinct differentiation trajectories (Figure 2C). Specifically examining the expression of globin genes, we found that as *HBB* expression declines during differentiation in HBBko cells as compared to WT, other globins become more highly expressed (Figure 2D).

Nonsense-induced transcriptional compensation (NITC) is a response to nonsense-mediated decay (NMD) of an important transcript and has emerged as a new mechanism for transcriptional reprogramming to upregulate related genes (El-Brolosy

upregulating what they can. This model is consistent with the phenomenon of increased γ-globin during cell-intrinsic erythroid stress and indicates that β$_0$-stress modeled by the HBBko line is useful to molecularly characterize this process.

### *HBB* Knockout Cells Reduce an ATF4-Mediated Transcriptional Response during Differentiation

Because *HBB* and *HBG* reciprocally regulated one another, we asked if *HBB* loss affects the transcription of other globins. We performed biological triplicate *in vitro* differentiation of paired WT and HBBko clones. RNA sequencing (RNA-seq) of terminally differentiated cells revealed widespread transcriptional alterations between WT and HBBko, with some of the largest fold changes being greatly reduced *HBB* and increased *HBG1*,

et al., 2019; Ma et al., 2019; Rossi et al., 2015). However, we found that knocking down the mRNA decay exonuclease XRN1 or the single-stranded RNA-binding protein SMG6 that are required for NITC had no effect on the upregulation of γ-globin in HBBko cells by intracellular FACS and qRT-PCR (Figure S2D).

We used pathway analysis to identify features in the RNA-seq data that could explain the transcriptional response in differentiated HBBko cells (Krämer et al., 2014). We found that ATF4 and 37 out of 40 ATF4 target genes were downregulated in HBBko cells relative to WT cells (Figures 2E and 2F).

ATF4 is a basic leucine zipper transcription factor associated with the integrated stress response (ISR) to unfolded proteins. ATF4 signaling decreases global protein synthesis while simultaneously inducing target genes. The downregulation of ATF4 and its ISR targets in HBBko cells was therefore surprising, since these cells harbor free α-globin aggregates that might have conversely initiated the ISR (Figure 1D) (Chen and Zhang, 2019). However, a focused CRISPR screen found that knockout of the known ATF4 upstream regulator HRI (heme-regulated eIF2α kinase) can induce moderate levels of HbF expression (Grevet et al., 2018). We hypothesized that both HBB and HRI knockout may induce globin synthesis by reducing ATF4 activity. This would mark ATF4 as a master regulator whose level maintains globin levels at homeostasis when a major globin becomes critically low.

## ATF4 Represses HbF Expression

By western blotting, we found that ATF4 levels are decreased in differentiated HBBko compared to WT cells (Figures 3A and S3A). ATF4 is itself positively regulated by phosphorylation of eIF2α via HRI. We also found decreased eIF2α phosphorylation (eIF2α-P) in HBBko cells (Figure 3A). These data further support our hypothesis that ATF4 and the ISR pathway are not upregulated by free α-globin aggregates in the context of HBBko cells. Instead, both HBB and HRI knockout may induce globin synthesis by reducing ATF4 activity.

To exclude the possibility of clonal effects during isolation of the HBBko clone, we tested whether ATF4 expression is decreased during bulk RNP knockout of HBB using a different guide RNA (e87; Figure 1B) than was used to generate HBBko. After bulk editing of HBB of HUDEP-2 cells using the e87 guide RNA and differentiation, we found decreased ATF4 expression and increased γ-globin by western blot (Figure S3B), qRT-PCR (Figure S3C), and flow cytometry (Figure S3D). We further tested whether the decrease in ATF4 after knockout of HBB was specific to loss of HBB or whether it applied to loss of other globins as well. For this, we utilized HUDEP-1 cells, which normally express high levels of HBG and no HBB (Kurita et al., 2013). We performed bulk HBG1/2 RNP knockout and observed a compensatory increase in β-globin by western blot (Figure S3E) but no difference in ATF4 expression. We note that basal ATF4 expression in untreated HUDEP-1 cells is low by western blot (Figure S3E), which is consistent with a model that low levels of ATF4 yields higher levels of γ-globin. Overall, this suggests that decrease of ATF4 expression is specific to loss of HBB. Loss of HBG likely engages different pathways to upregulate HBB, and whether these pathways are also involved in loss of HBB is currently unknown.

Taken together, our data suggest that reduction of β-globin leads to a decrease in ATF4 expression via a paradoxical reduction of eIF2α signaling. Reduced ATF4 leads to high levels of γ-globin in the context of HBB knockout.

Next, we developed two CRISPR-Cas9 genome editing strategies to further assess whether ATF4 was involved in globin homeostasis, specifically in fetal globin regulation, in cells that predominantly express adult globin. First, we used a dual-guide approach to excise the entirety of the ATF4 gene, starting from the WT HUDEP-2 clone (Figure S3F). Two ATF4 knockout clones resulting from total excision were named ATF4ko-1 and ATF4ko-2 (Figure S3G). The knockout clones showed successful knockout of ATF4 by western blotting, with no protein detected even after treatment with cyclopiazonic acid (CPA), a drug that increases ATF4 expression through induction of endoplasmic reticulum (ER) stress (Figure S3H). Notably, ATF4ko-1 and ATF4ko-2 were unable to undergo in vitro differentiation and instead exhibited extensive cell death after 5 days in differentiation media (Figure S3I). This suggests that complete loss of ATF4 is not well tolerated and is consistent with a known role of ATF4 as essential in erythroid differentiation (Masuoka and Townes, 2002; Suragani et al., 2012; Zhang et al., 2019).

Second, we explored N-terminal truncation mutants of ATF4 with separation-of-function properties (Steinmüller and Thiel, 2003). We found that dual guides targeted to remove most of the first exon of ATF4 (Figure S3F) lead to reinitiation of translation at the next ATG in the second exon. This produces a stable protein fragment of ∼30 kDa lacking the N-terminal regulatory region but retaining the C-terminal dimerization and DNA-binding domain (Figure S3H). We derived an edited clone from WT HUDEP-2 s using the above strategy, naming it ATF4-ΔN (Figure S3G). By ChIP-qPCR, we found that ATF4ΔN still binds the ASNS promoter, but qRT-PCR indicated that ATF4-ΔN does not support transcription of ASNS (Figure S3J). ATF4-ΔN was more highly expressed than WT ATF4 and no longer induced by ER stress (Figure S3H). However, this may be offset by the loss of ATF4ΔN's transcriptional activation activity. By contrast to ATF4ko-1 and ATF4ko-2, the ATF4ΔN clone was still able to successfully differentiate as measured by high live-cell numbers and successful globin expression after 5 days of culture in differentiation media (Figures S3I and S3M). ATF4 has been found to heterodimerize with other transcription factors, such as CCAAT-enhancer-binding proteins (CEBPs) (Su and Kilberg, 2008). Therefore, while ATF4ΔN may have reduced transcriptional activity, retention of ATF4's heterodimer partner activity could be sufficient for cell differentiation.

We tested the globin status of the ATF4ko and ATF4ΔN cell lines. Undifferentiated ATF4ko and ATF4ΔN cells expressed normal levels of β-globin and slightly increased γ-globin by intracellular FACS (Figures 3B and S3L) and western blot (Figure 3C). Strikingly, in vitro differentiation of ATF4ΔN led to high levels of transcripts for HBB, HBE, HBZ, and HBG (Figure S3M). This was reflected in increased γ-globin by intracellular FACS (Figures 3D and S3K). The global upregulation of globin expression with especially high levels of γ-globin upon differentiation of ATF4ΔN mirrors the response in differentiated HBB knockout cells. These data indicate that ATF4 is involved in repressing HbF in the undifferentiated state, and a lack of ATF4
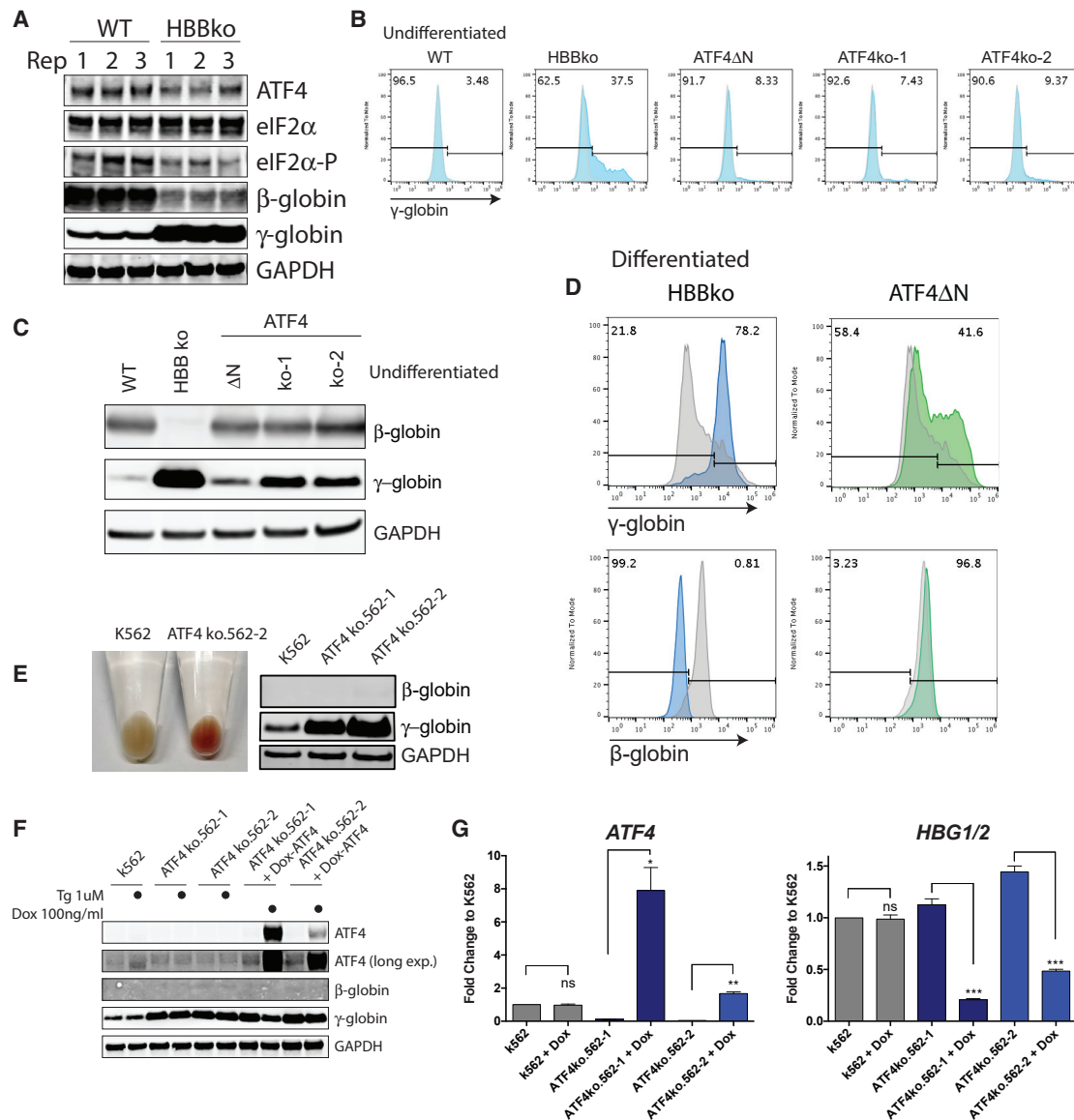
**Figure 3. Endogenous Mutation of ATF4 Leads to Increased γ-Globin in HUDEP-2 and K562 Cells**

(A) Western blot of 5-day-differentiated WT and HBBko showing ATF4, eIF2α, eIF2α-P, β-globin, and γ-globin. Biological triplicates are shown. Quantification is shown in Figure S3A.

(B) Intracellular FACS for γ-globin of undifferentiated HUDEP-2 cells comparing WT, HBBko, and ATF4 clones. Biological quadruplicates are quantified and shown in Figure S3L.

(C) Western blot of undifferentiated WT, HBBko, and ATF4 mutant cells showing β-globin and γ-globin levels.

(D) Intracellular FACS for γ-globin of differentiated HBBko and ATF4ΔN cells as compared to WT (trace in gray). Biological triplicates are quantified in Figure S3K.

(E) Left: cell pellets from WT K562 and ATF4ko K562 cells. Right: western blot for β-globin and γ-globin in WT and ATF4ko K562 clones. qRT-PCR confirmed loss of *ATF4* transcript in ATF4ko clones and increased *HBG1/2* (Figure S3N).

(F) Western blot of k562 cells and ATF4ko.562-1,2 with doxycycline-inducible ATF4 constructs treated with 1 μM thapsigargin or 100 ng/mL doxycycline for 48 h showing ATF4, β-globin, and γ-globin.

(G) qRT-PCR of *ATF4* and *HBG1/2* in k562 cells and ATF4ko.562-1/2 cells. ATF4ko.562-1/2 have stable expression of doxycycline-induced *ATF4* transgene. Cells were treated with 100 ng/mL doxycycline for 48 h. The data are presented as mean ± SD of three biological replicates. p value indicates paired, two-tailed Student's t test (ns, nonsignificant; *p ≤ 0.05; **p ≤ 0.01; ***p ≤ 0.001).

signaling in the differentiated state leads to upregulation of multiple globins that mimics the response to lack of *HBB*.

The ability of *ATF4* knockout or ATF4ΔN clones to modestly upregulate HbF in the undifferentiated state prompted us to

ask whether ATF4 is involved in basal HbF repression in other cell types. We used CRISPR-Cas9 to remove the entire *ATF4* gene from K562 erythroleukemia cells, which normally express no β-globin and moderate levels of γ-globin. We generated
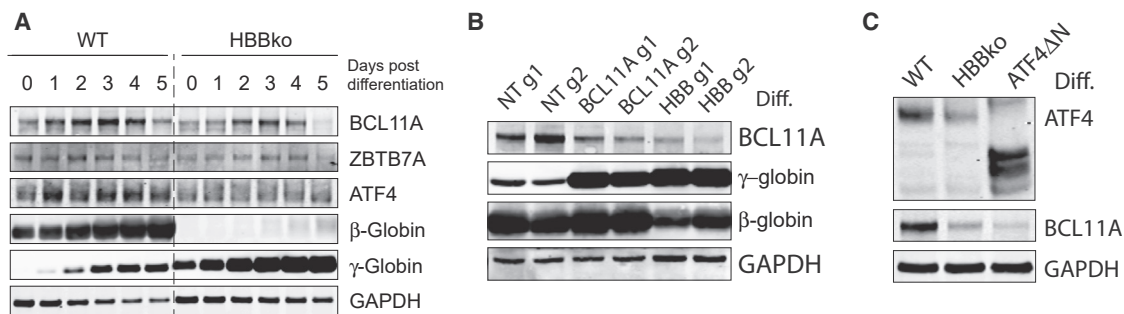
**Figure 4. Loss of β-Globin or ATF4 Downregulates BCL11A**

(A) Western blot of HBBko and WT cells over the course of differentiation showing BCL11A, ZBTB7A, ATF4, β-globin, and γ-globin.

(B) Western blot of 5-day-differentiated HUDEP-2 cells showing CRISPRi knockdown efficiency of BCL11A and β-globin, as well as resulting increases in γ-globin protein.

(C) Western blot of 5-day-differentiated WT, HBBko, and ATF4ΔN comparing BCL11A levels.

two different *ATF4* knockout K562 cell lines that we termed ATF4ko.562-1 and ATF4ko.562-2 using an analogous protocol as for the HUDEP-2 ATF4 knockout lines (Figure S3F). We found that both K562 *ATF4* knockout lines became strikingly red and expressed very high levels of γ-globin but still failed to express β-globin (Figure 3E), even when they were maintained in undifferentiated culture conditions.

We next tested whether overexpression of *ATF4* is sufficient to prevent upregulation of HbF. We attempted to overexpress *ATF4* in HUDEP-2 cells but were unsuccessful, as high levels of ATF4 were not well tolerated and induced cell death in this model (data not shown). Instead, we stably expressed a doxycycline-inducible *ATF4* construct in *ATF4* knockout K562 cells, which basally express high levels of γ-globin. This construct could not be used in HUDEP-2 cells, which require doxycycline in their media. We found that 48 h of doxycycline treatment led to high levels of ATF4 and decreased γ-globin and *HBG* transcript levels by western blot (Figure 3F) and qRT-PCR, respectively (Figure 3G).

### Loss of ATF4 Downregulates BCL11A

As a transcription factor, ATF4 could directly or indirectly regulate the expression of *HBG1/2* and other globins. BCL11A and ZBTB7A (also known as LRF) are two transcriptional repressors that directly repress fetal globin expression after birth. We asked whether BCL11A and ZBTB7A are misregulated in our *HBB* knockout model of β_0-stress or after loss of ATF4.

Examining the WT and HBBko time-course differentiation RNA-seq data, we found that *ATF4* transcripts were much lower in HBBko in the undifferentiated state but stabilized to WT levels after 5 days of differentiation. The expression of both *BCL11A* and *ZBTB7A* were reduced in the HBBko line, with BCL11A expression declining during differentiation and ZBTB7A remaining at a consistent reduced level (Figure S4A). This corresponded to reduced expression of BCL11A protein in HBBko during differentiation (Figure 4A). A decrease in BCL11A also provides a potential explanation for the observed increase in embryonic globin transcripts in the HBBko line, as BCL11A binds to the *HBE* and *HBZ* promoters (Liu et al., 2018; Xu et al., 2010).

Stable CRISPRi knockdown of BCL11A resulted in similar increases in γ-globin to knockdown of *HBB*, as measured by FACS (Figure S4B). Knockout or knockdown of *HBB* also both led to a decrease in BCL11A by western blot (Figure 4B). In the undifferentiated state, the ATF4ΔN and ATF4ko-1 and ATF4ko-2 expressed normal levels of BCL11A and ZBTB7A (Figure S4C). However, after differentiation, the ATF4ΔN clone exhibited lower levels of BCL11A protein (Figure 4C). *HBB* knockout and reduced ATF4 signaling might therefore increase γ-globin expression by directly or indirectly reducing levels of BCL11A during differentiation. However, this is at odds with data from K562 cells, which do not express BCL11A (Figure S4D) yet dramatically increase *HBG* upon knockout of *ATF4* (Figure 3D).

### ATF4 Binding Is Attenuated in HBBko Cells Relative to WT

To test whether ATF4 is directly involved in transcriptional regulation of BCL11A, we performed endogenous ATF4 ChIP-seq in various HUDEP-2 genetic backgrounds and differentiation states to map ATF4 targets during hemoglobinization. In the undifferentiated state, we performed ATF4 ChIP-seq in WT, HBBko, and ATF4ko (negative control) clones. After 5 days of *in vitro* differentiation, we performed ATF4 ChIP-seq in WT and HBBko clones and with an immunoglobulin G (IgG) isotype negative control in the WT clone (since the ATF4ko clone cannot be differentiated). We also performed ATF4 and IgG ChIP-seq in the differentiated ATF4ΔN clone, which verified that this ATF4 mutant retains a WT binding profile on a genome-wide level (Figure S5A). Lastly, we performed ATF4 ChIP-seq on human CD34^{+} derived early and late erythroblasts, with IgG as a negative control.

The overall number of ATF4 binding sites increased upon differentiation in both primary human erythroblasts as well as differentiated HUDEP-2 cells. (Figures 5A and S5B). This increase in ATF4 binding further highlights the importance of ATF4 signaling during erythroid differentiation.

Between all four experimental conditions in isogenically controlled HUDEP-2 cells (WT undifferentiated, HBBko undifferentiated, WT differentiated, and HBBko differentiated), we found 1,245 unique ATF4 ChIP-seq peaks with an irreproducible discovery rate (IDR) >2% and a signal value >30 over background (ATF4 knockout or IgG control). Bona fide ATF4 binding sites showed high read count and clear enrichment over background
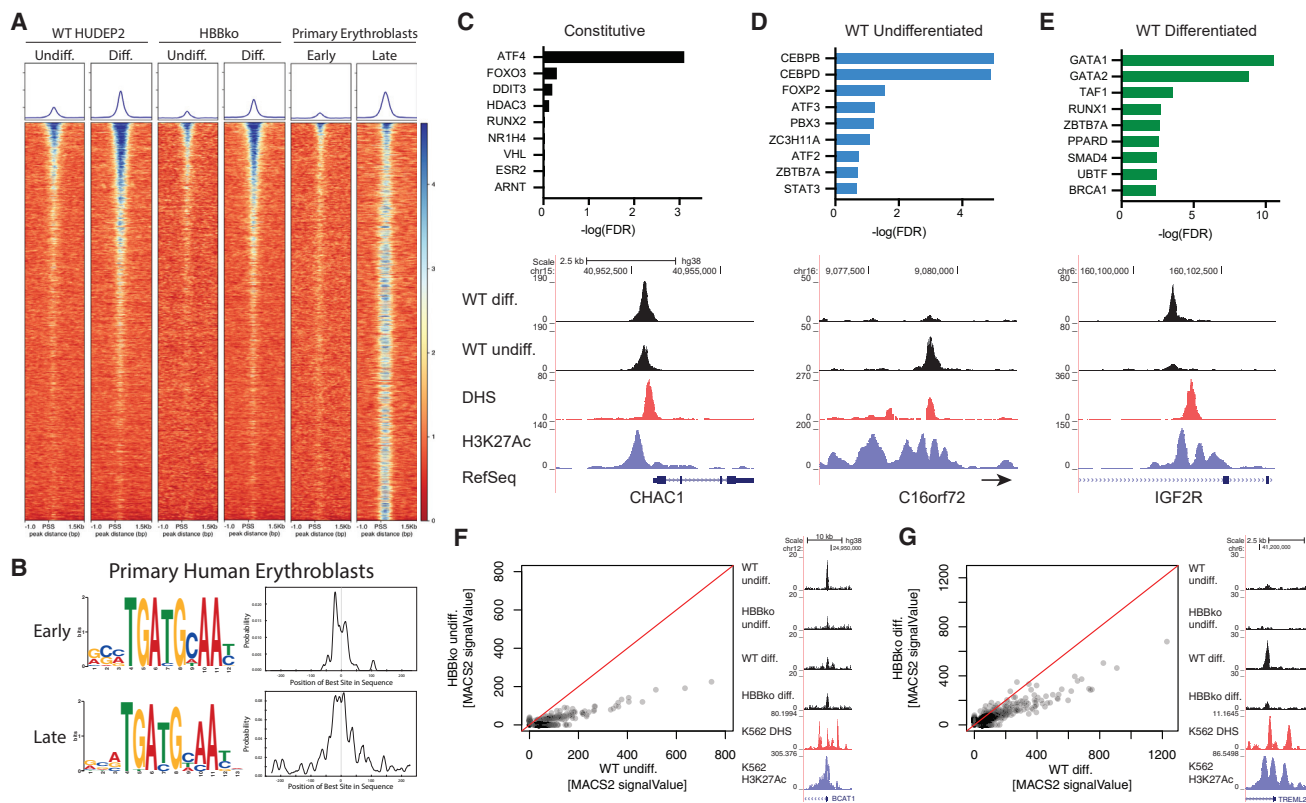
**Figure 5. ATF4 Signaling Is Attenuated in HBBko Cells**

(A) Heatmap of ATF4 ChIP-seq showing fold change over each respective control for all peaks across samples. Differentiation increases ATF4 occupancy at most identified binding sites.

(B) Unbiased motif discovery on ATF4 ChIP-seq in primary human early erythroblasts identifies the ATF4 consensus sequence.

(C) Unbiased enrichment analysis of ATF4 ChIP-seq peaks present in both the undifferentiated and differentiated states against databases of transcription factor targets. Example ATF4 ChIP-seq profiles are shown below, together with reference ENCODE DNaseI hypersensitivity and H3K27Ac data. Lack of ATF4 signal at the globin, *BCL11A*, and *ZBTB7A* loci is shown in Figures S6D–S6F.

(D) Unbiased enrichment analysis of ATF4 ChIP-seq peaks present in only the undifferentiated state.

(E) Unbiased enrichment analysis of ATF4 ChIP-seq peaks present in only the differentiated state.

(F) MACS2 signal value for all ATF4 ChIP-seq peaks comparing WT to HBBko cells in the undifferentiated state. Example ATF4 ChIP-seq profiles are shown to the right of each global ChIP-seq comparison.

(G) MACS2 signal value for all ATF4 ChIP-seq peaks comparing WT to HBBko cells in the differentiated state.

(e.g., up to 255 reads and 85-fold enrichment at ASNS). Unbiased motif discovery on these ChIP-seq peaks identified a central ATF4 consensus site (Figures 5B and S5C), verifying the quality of the datasets. Cross-comparison with our time-course RNA-seq data revealed that ATF4 binding was associated with a subset of well-expressed genes, and less ATF4 binding was present at lowly expressed genes. This further indicates that the identified ATF4 sites are involved in active transcription (Figure S5D).

We used the four isogenically controlled HUDEP-2 ChIP-seq datasets to identify new ATF4 binding sites that varied depending on differentiation status and HBB genotype. Unbiased enrichment analysis against databases of transcription factor targets or transcription factor ChIP-seq (Huang et al., 2009; Kuleshov et al., 2016) revealed clear patterns for several distinct categories of ATF4 ChIP-seq peaks.

"Constitutive" ATF4 sites were defined as present regardless of differentiation status in both WT and HBBko. Constitutive

peaks were dominated by an ATF4 signal, validating our set of ChIP-seq experiments against datasets in other cell contexts (Figures 5C and S5E). "WT undifferentiated" ATF4 sites were defined as at least 2-fold enriched in WT cells in the undifferentiated state and not found in the differentiated state. WT undifferentiated peaks were highly represented at targets and binding sites of ATF4 partners that either form bZIP heterodimers with ATF4 (e.g., CEBPs) or are part of the same family as ATF4 (e.g., ATF3) (Figures 5D and S5F). "WT differentiated" ATF4 sites were defined as at least 2-fold enriched in WT cells in the differentiated state and not found in the undifferentiated state. WT differentiated peaks were unexpectedly represented at targets and binding sites of transcription factors involved in hematopoietic differentiation (e.g., GATA1/2 and ZBTB7A) but with no known ATF4 partnership (Figures 5E and S5G).

ATF4 binding to GATA1 target genes implies that ATF4 cooperates with hematopoietic differentiation transcription factors at their target genes, providing a rationale for ATF4's requirement
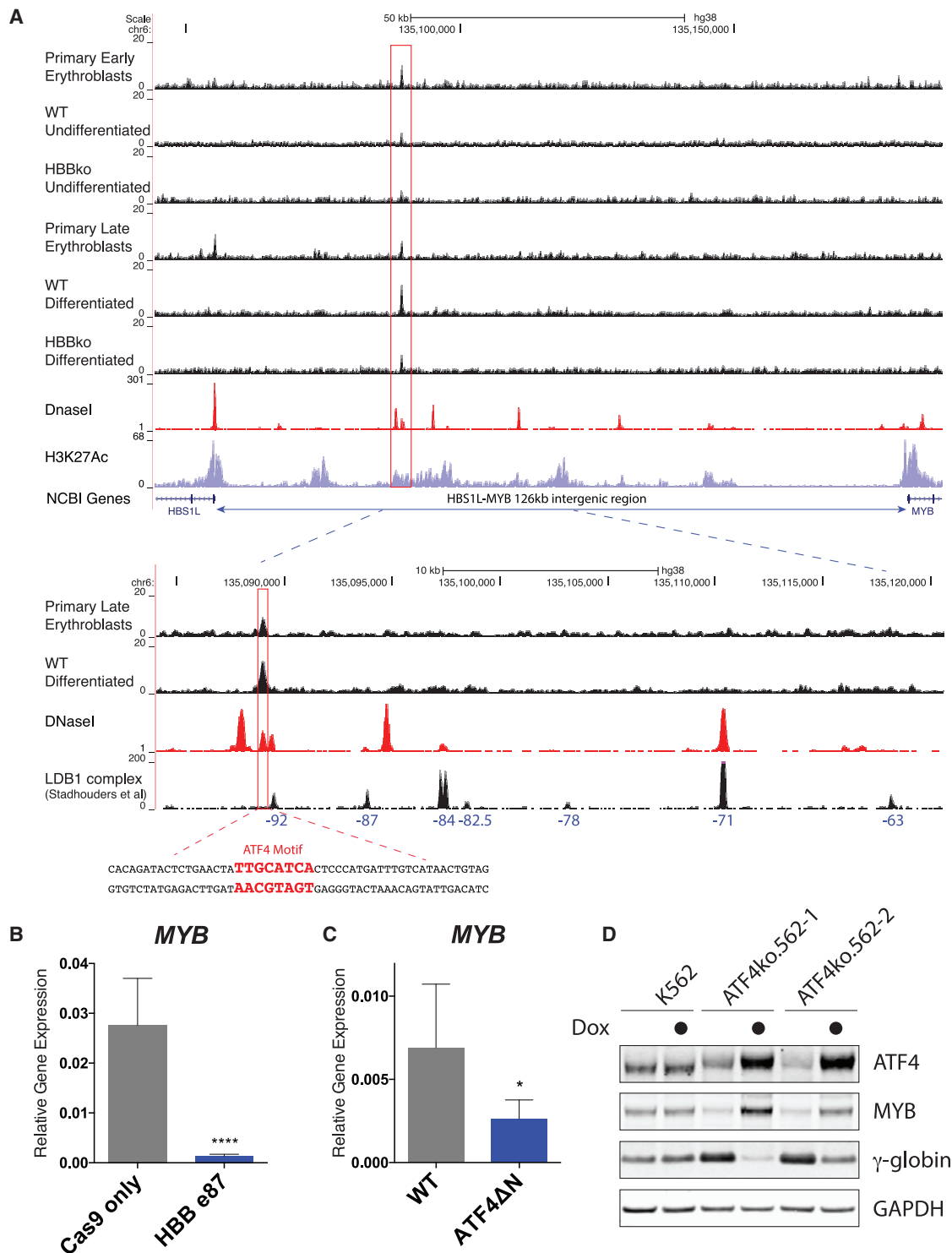
**Figure 6. ATF4 Regulation within the *HBS1L-MYB* Intergenic Enhancer Region**

(A) Top: ATF4 ChIP-seq tracks at the *HBS1L-MYB* intergenic enhancer region. An ATF4 peak is boxed in red. DNaseI track is from previously published data in CD34^{+} primary cells (Neph et al., 2012). H3K27Ac track is from previously published primary erythroblasts (Xu et al., 2012). Bottom: zoomed in ATF4 ChIP-seq tracks along with previously published LDB1 complex ChIP-seq track (Stadhouders et al., 2014). Numbers in blue correspond to characterized LDB1 regulatory regions and indicate the number of kilobases upstream of the *MYB* gene (Stadhouders et al., 2014). An ATF4 peak containing an ATF4 consensus motif is boxed in red.

*(legend continued on next page)*

during hematopoietic differentiation. We compared our ATF4 ChIP-seq data to GATA1 ChIP-seq in primary human erythroblasts (Dunham et al., 2012) and identified 753 cases in which ATF4 and GATA1 peaks are associated with the same gene and are within 10 kb of one another (Figure S76A). Some of these were cases of nonoverlapping regulatory regions in which the same genomic target was associated with distinct ATF4 and GATA1 peaks. A large proportion of putative co-regulatory sites involved overlap between the ATF4 and GATA1 ChIP-seq signal (371 of 2,766 total ATF4 peaks [13.41%]) (Figure S7A). Performing motif analysis with the ATF4 ChIP-seq peaks as an anchor, we found that overlapping sites frequently harbor a GATA1 consensus motif either underneath or immediately adjacent to the ATF4 peak (Figure S6B). Taken together, these data suggest that ATF4 has unappreciated regulatory functions that overlap those of the GATA1 hematopoietic transcription factor, and highlight the importance of ATF4 in erythroid differentiation.

Returning to the role of ATF4 in loss of *HBB*, we found that ChIP-seq signal at ATF4 binding sites was attenuated in HBBko cells relative to WT in both the differentiated and undifferentiated states (Figures 5F and 5G). Binding of ATF4 was particularly reduced at several genes involved in the unfolded protein response and feedback regulators of ATF4 (e.g., XBP1, HSPA5/BiP, CREB3L1, EDEM1, ATF3, ATF6, RACK1, SEL1L, and TRIB3). Many of these factors are not canonical ATF4 targets, but their expression levels were also reduced in RNA-seq of differentiating HBBko cells (Figure S6C). These data are consistent with downregulation of ATF4 levels and signaling in HBBko cells, despite increased α-globin aggregates in HBBko cells.

### ATF4 Binds the *HBS1L-MYB* Intergenic Enhancer Region and Regulates *MYB* Expression

We were surprised to find no evidence of ATF4 binding anywhere in the vicinity of the globin locus, *BCL11A*, or *ZBTB7A*, including all known promoters and enhancers (Figures S6D–S6F). This was true of all cells tested, regardless of genotype and whether they were HUDEP-2 cells or CD34+-derived erythroblasts. Upon further investigation, we instead found evidence of ATF4 binding at an ATF4 consensus motif within the *HBS1L-MYB* intergenic enhancer region (Figure 6A). This enhancer region is known to regulate fetal globin expression, and MYB is an essential transcription factor for erythropoiesis and hematopoiesis that regulates fetal globin, *BCL11A*, and *ZBTB7A* (Bianchi et al., 2010; Cavazzana et al., 2017; Jiang et al., 2006; Lettre et al., 2008; Stadhouders et al., 2014; Thein et al., 2007; Wang et al., 2018). The LDB1 erythroid transcription factor complex, which contains GATA1 (Soler et al., 2010), acts on the *HBS1L-MYB* intergenic region at multiple sites (Stadhouders et al., 2014). The ATF4 peak identified here overlaps a DNaseI hypersensitive site and is directly adjacent to the −92 LDB1 site (Figure 6A). This adja-

cency of an ATF4 peak to an LDB1 complex site in the *HBS1L-MYB* intergenic region provides specific context to the global co-occurrence of ATF4 and GATA1 peaks highlighted earlier (Figures 5E, S6A, and S6B).

Having identified a previously unappreciated ATF4 binding site in a known *MYB* regulatory region, we asked whether ATF4 levels and the loss of *HBB* affect *MYB*. Indeed, *MYB* expression was greatly decreased after bulk Cas9 editing of *HBB* and differentiation of HUDEP-2 cells (Figure 6B). *MYB* expression was also decreased in differentiated ATF4ΔN HUDEP-2 cells as compared to WT (Figure 6C) and in ATF4 knockout K562 cells (Figure 6E). Significantly, doxycycline-induced expression of a stable *ATF4* transgene rescued *MYB* in the ATF4 knockout background (Figure S6G). By western blot, we observed that MYB was downregulated in ATF4 knockout cells, and overexpression of ATF4 rescued MYB levels while decreasing γ-globin (Figure 6D). Since K562 cells do not express BCL11A, involvement of the upstream multifunctional regulator *MYB* potentially explains how loss of ATF4 leads to upregulation of fetal globin in this context. Taken together, our data indicate that reduced ATF4 upregulates fetal globin through direct regulation of *MYB* and indirect regulation of *BCL11A*.

### DISCUSSION

Stress erythropoiesis results from a high erythropoietic drive and is induced during anemias such as β-thalassemia. Cell-intrinsic erythroid stress leads to upregulation of γ-globin, but the pathways that mediate this phenomenon have remained unclear. We found that $β_0$-stress caused by loss of β-globin in erythroid precursors induces ATF4-mediated reprogramming that includes upregulation of several globins, including very high levels of γ-globin. ATF4 signaling is required to maintain levels of BCL11A during differentiation, but ATF4 surprisingly does not bind *BCL11A* or *ZBTB7A* or the globin locus. Instead, our data support a model in which reduced ATF4 signaling during $β_0$-stress regulates γ-globin levels via *MYB*.

Translation of ATF4 mRNA is regulated by phosphorylation of eIF2α, which is itself activated by several different kinases, including HRI (Chen, 2014). Upon stress, the HRI pathway will inhibit protein synthesis, which then promotes efficient translation of ATF4 mRNA. Knockout of *HRI* was reported to decrease expression of BCL11A and increase expression of *HBG* (Grevet et al., 2018). However, the link between HRI and BCL11A remained undetermined. Our data suggest that a lack of HRI leads to decreased eIF2α-phosphorylation and reduction of ATF4 activity, similar to what we observe for knockout of *HBB*. Deletions of *HRI*, *HBB*, and *ATF4* all lead to reduced BCL11A.

While our manuscript was under revision, a transcription-factor-focused CRISPR screen found that knockout of ATF4 upregulates gamma globin (Huang et al., 2020). Our own work reveals

---

(B) qRT-PCR for *MYB* expression in bulk-edited and differentiated HUDEP-2 cells using guide *HBB* e87. The data are presented as mean ± SD of six biological replicates. p value indicates unpaired, two-tailed Student's t test (****p ≤ 0.0001).

(C) qRT-PCR for *MYB* expression in differentiated ATFΔN compared to WT cells. The data are presented as mean ± SD of three biological replicates. p value indicates paired, two-tailed Student's t test (*p ≤ 0.05).

(D) Western blot of K562 and ATF4 knockout cells with a doxycycline-inducible ATF4 transgene showing ATF4, MYB, and γ-globin. Cells were treated with or without 50 ng/mL doxycycline for 5 days.

why ATF4 might be reduced in the first place, and together, the two results independently highlight ATF4 as a regulator of globin expression. In contrast to our results, the other study found evidence for ATF4 binding within the *BCL11A* +55 enhancer. While we originally hypothesized that ATF4 directly regulates BCL11A, none of our carefully controlled ATF4 ChIP-seq datasets in multiple genetic backgrounds and cell types supported this hypothesis. Additionally, given that knockout of ATF4 increases $\gamma$-globin in K562 cells that do not express BCL11A, ATF4-mediated regulation of $\gamma$-globin must not be solely dependent upon BCL11A. Our data instead show that ATF4 binds the *HBS1L-MYB* intergenic enhancer region, adjacent to an LDB1 erythroid complex binding site. ATF4 binding at the *HBS1L-MYB* intergenic enhancer is also present, but not commented upon, in the ChIP-seq data from the study that suggested direct regulation of *BCL11A* by ATF4 (Huang et al., 2020). Notably, ATF4 binds to the BCL11A intronic enhancer in both human and mouse cells, but ATF4 only regulates $\gamma$-globin in human cells (Huang et al., 2020). Mice harbor several mutations that disrupt the human *HBS1L-MYB* intergenic region ATF4 motif, and ATF4 does not bind the intergenic region in murine G1-ER4 cells by ChIP-seq (Huang et al., 2020).

In human cells, we found that levels of MYB are responsive to both *HBB* status and *ATF4* genotype. *MYB* is a known regulator of fetal globin on multiple levels, including *BCL11A* and *ZBTB7A* (Bianchi et al., 2010; Cavazzana et al., 2017; Stadhouders et al., 2014; Wang et al., 2018). We therefore suggest an alternative model in which ATF4 directly regulates *MYB* to indirectly regulate $\gamma$-globin. Follow-up experiments will be needed to further unravel the connections between ATF4 and MYB, as well as to test the differential activity of the ATF4 upon *MYB* in mouse models.

We found that knockout of *HBB* or *ATF4* leads to upregulation of multiple globins, with *HBG1/2* exhibiting the largest change, as well as reductions in almost all known ATF4 targets. Overall, this suggests that ATF4 signaling in response to loss of $\beta$-globin is part of a larger program to maintain high globin levels in differentiating erythroid cells. The response to loss of $\beta$-globin could include HRI-like signaling as well as additional facets. Knockout of *HRI* has been suggested as a strategy to ameliorate anemic disorders via re-expression of HbF (Grevet et al., 2018). Indeed, knockout or CRISPRi of *HBB* leads cells to express remarkable levels of *HBG1/2*, but the broad roles of ATF4 in processes other than erythropoiesis also suggest that this strategy should be pursued with caution.

The HRI-eIF2$\alpha$P-ATF4 axis represses globin synthesis under low-heme or low-iron conditions in order to keep excess globins in line with the availability of cofactors (Chen and Zhang, 2019; Crosby et al., 2000; Suragani et al., 2012). Unfolded proteins such as $\alpha$-globin aggregates can also activate HRI-eIF2$\alpha$P-ATF4, leading to the ISR and repression of protein synthesis. ATF4 downstream of reduced *HBB* could therefore either be activated by an unfolded protein response or attenuated by reduced HRI activity caused by excess heme. While knockout of *HBB* leads to the formation of $\alpha$-globin aggregates, we paradoxically found that ATF4 signaling is reduced. This suggests that excess heme remaining after loss of *HBB* and intact HbA plays a dominant role over $\alpha$-globin aggregates to reduce ATF4 activity. Indeed, supplementing K562 cells with hemin leads to a reduction in MYB (Fuglerud et al., 2017). We found

that lowered ATF4 activity reactivates globin synthesis, and the formation of HbF could reduce the burden of accumulating $\alpha$-globin aggregates to allow coordination of cofactors and a return to homeostasis. Our findings demonstrate that the HRI-eIF2$\alpha$P-ATF4 ISR is involved in adaptation to loss of HBB and that downregulation of the ISR induces embryonic and fetal globin gene transcription. Downregulation of ISR by stress recovery has also been found to increase the translational efficiency of $\beta$-globin and $\gamma$-globin (Hahn and Lowrey, 2014). Taken together, the ISR works cooperatively to increase $\beta$-like globin production during $\beta_0$-stress.

The dramatic increase in $\gamma$-globin caused by *ex vivo* reduction in *HBB* raises the question of why $\beta$-thalassemia phenotypes are not always ameliorated by ATF4-mediated globin compensation. $\beta$-Thalassemia patients can express high levels of HbF over long periods of time (Galanello et al., 1989; Manca and Masala, 2008; Rochette et al., 1994), but this phenomenon is not ubiquitous. Mouse models have indicated that the HRI-eIF2$\alpha$P-ATF4 axis is protective against some forms of $\beta$-thalassemia, at least in part by upregulating fetal globin (Han et al., 2005; Suragani et al., 2012). This is at odds with observations that knockout of *HRI* is protective against sickle cell anemia phenotypes by inducing HbF (Grevet et al., 2018) and our own data that knockout of ATF4 or reductions in ATF4 levels downstream of *HBB* knockout both induce high levels of HbF. Since HRI-eIF2$\alpha$P-ATF4 is involved in the ISR in all cells, reductions in this signaling axis might be negatively selected for during development or otherwise compensated in individuals with $\beta$-thalassemia. In this case, developing a cell-type-specific approach to disrupting the HRI-eIF2$\alpha$P-ATF4 axis after birth (e.g., during *ex vivo* editing of HSPCs) could be an important avenue for the treatment of hemoglobinopathies. The molecular pathways we find at work during *ex vivo* culture could also be quite different during long-term function *in vivo*. We previously observed high levels of HbF in *HBB*-edited long-term hematopoietic stem cells (LT-HSCs) recovered after 4 months of xenotransplantation in NBSGW mice (https://www.biorxiv.org/content/10.1101/432716v6), but this does not conclusively address long-term function in an individual with $\beta$-thalassemia. Determining the long-term roles of the HRI-eIF2$\alpha$P-ATF4 axis in patient HSPCs will be an important future step to further unraveling the mechanisms of stress erythropoiesis.

## STAR★METHODS

Detailed methods are provided in the online version of this paper and include the following:

- KEY RESOURCES TABLE
- RESOURCE AVAILABILITY
  - Lead Contact
  - Material Availability
  - Data and Code Availability
- EXPERIMENTAL MODEL AND SUBJECT DETAILS
  - Cell Lines
  - K562 cell culture
  - HEK293T cell culture
  - Primary Cell Cultures

- METHOD DETAILS
  - ○ Generation of CRISPRi HUDEP-2 cells
  - ○ Lenti-viral Packaging
  - ○ sgRNA Plasmid Cloning
  - ○ Cas9 RNP Nucleofection
  - ○ IVT sgRNA
  - ○ High Pressure Liquid Chromatography and Mass Spectrometry
  - ○ Intracellular FACs Staining
  - ○ RNA-Seq
  - ○ qRT-PCR
  - ○ ChIP-qPCR
  - ○ ChIP-seq
  - ○ Western Blot
- QUANTIFICATION AND STATISTICAL ANALYSIS

**SUPPLEMENTAL INFORMATION**

Supplemental Information can be found online at https://doi.org/10.1016/j.celrep.2020.107993.

**AUTHOR CONTRIBUTIONS**

M.Y.B. and J.E.C. designed the experiments. M.Y.B., G.M.S., M. Banović, R.J.L., M. Bordi, B.G.G., and M.A.D. performed experiments. M.Y.B., M.S.S., S.K.W., and J.E.C. analyzed data. M.Y.B. and J.E.C. wrote the manuscript. All authors contributed feedback for the manuscript.

**DECLARATION OF INTERESTS**

The authors declare no competing interests.

**REFERENCES**

Alter, B.P. (1979). Fetal erythropoiesis in stress hematopoiesis. Exp. Hematol. 7 (Suppl 5), 200–209.

Amemiya, H.M., Kundaje, A., and Boyle, A.P. (2019). The ENCODE blacklist: identification of problematic regions of the genome. Sci. Rep. 9, 9354.

Antoniani, C., Romano, O., and Miccio, A. (2017). Concise Review: Epigenetic regulation of hematopoiesis: biological insights and therapeutic applications. Stem Cells Transl. Med. 6, 2106–2114.

Bauer, D.E., Kamran, S.C., Lessard, S., Xu, J., Fujiwara, Y., Lin, C., Shao, Z., Canver, M.C., Smith, E.C., Pinello, L., et al. (2013). An erythroid enhancer of

BCL11A subject to genetic variation determines fetal hemoglobin level. Science 342, 253–257.

Berry, M., Grosveld, F., and Dillon, N. (1992). A single point mutation is the cause of the Greek form of hereditary persistence of fetal haemoglobin. Nature 358, 499–502.

Bianchi, E., Zini, R., Salati, S., Tenedini, E., Norfo, R., Tagliafico, E., Manfredini, R., and Ferrari, S. (2010). c-myb supports erythropoiesis through the transactivation of KLF1 and LMO2 expression. Blood 116, e99–e110.

Bray, N.L., Pimentel, H., Melsted, P., and Pachter, L. (2016). Near-optimal probabilistic RNA-seq quantification. Nat. Biotechnol. 34, 525–527.

Cavazzana, M., Antoniani, C., and Miccio, A. (2017). Gene therapy for β-hemoglobinopathies. Mol. Ther. 25, 1142–1154.

Chen, J.J. (2014). Translational control by heme-regulated eIF2α kinase during erythropoiesis. Curr. Opin. Hematol. 21, 172–178.

Chen, J.J., and Zhang, S. (2019). Heme-regulated eIF2α kinase in erythropoiesis and hemoglobinopathies. Blood.

Chung, J.E., Magis, W., Vu, J., Heo, S.J., Wartiovaara, K., Walters, M.C., Kurita, R., Nakamura, Y., Boffelli, D., Martin, D.I.K., et al. (2019a). CRISPR-Cas9 interrogation of a putative fetal globin repressor in human erythroid cells. PLoS ONE 14, e0208237.

Chung, J.E., Magis, W., Vu, J., Heo, S.J., Wartiovaara, K., Walters, M.C., Kurita, R., Nakamura, Y., Boffelli, D., Martin, D.I.K., et al. (2019b). CRISPR-Cas9 interrogation of a putative fetal globin repressor in human erythroid cells. PLoS ONE 14, e0208237.

Crosby, J.S., Chefalo, P.J., Yeh, I., Ying, S., London, I.M., Leboulch, P., and Chen, J.J. (2000). Regulation of hemoglobin synthesis and proliferation of differentiating erythroid cells by heme-regulated eIF-2α kinase. Blood 96, 3241–3248.

DeWitt, M.A., Magis, W., Bray, N.L., Wang, T., Berman, J.R., Urbinati, F., Heo, S.J., Mitros, T., Muñoz, D.P., Boffelli, D., et al. (2016). Selection-free genome editing of the sickle mutation in human adult hematopoietic stem/progenitor cells. Sci. Transl. Med. 8, 360ra134.

Dunham, I., Kundaje, A., Aldred, S.F., Collins, P.J., Davis, C.A., Doyle, F., Epstein, C.B., Frietze, S., Harrow, J., Kaul, R., et al.; ENCODE Project Consortium (2012). An integrated encyclopedia of DNA elements in the human genome. Nature 489, 57–74.

El-Brolosy, M.A., Kontarakis, Z., Rossi, A., Kuenne, C., Günther, S., Fukuda, N., Kikhi, K., Boezio, G.L.M., Takacs, C.M., Lai, S.L., et al. (2019). Genetic compensation triggered by mutant mRNA degradation. Nature 568, 193–197.

Fuglerud, B.M., Lemma, R.B., Wanichawan, P., Sundaram, A.Y.M., Eskeland, R., and Gabrielsen, O.S. (2017). A c-Myb mutant causes deregulated differentiation due to impaired histone binding and abrogated pioneer factor function. Nucleic Acids Res. 45, 7681–7696.

Galanello, R., Barella, S., Maccioni, L., Paglietti, E., Melis, M.A., Rosatelli, M.C., Argiolu, F., and Cao, A. (1989). Erythropoiesis following bone marrow transplantation from donors heterozygous for β-thalassaemia. Br. J. Haematol. 72, 561–566.

Gowen, B.G., Chim, B., Marceau, C.D., Greene, T.T., Burr, P., Gonzalez, J.R., Hesser, C.R., Dietzen, P.A., Russell, T., Iannello, A., et al. (2015). A forward genetic screen reveals novel independent regulators of ULBP1, an activating ligand for natural killer cells. eLife 4, 4.

Grant, C.E., Bailey, T.L., and Noble, W.S. (2011). FIMO: scanning for occurrences of a given motif. Bioinformatics 27, 1017–1018.

Grevet, J.D., Lan, X., Hamagami, N., Edwards, C.R., Sankaranarayanan, L., Ji, X., Bhardwaj, S.K., Face, C.J., Posocco, D.F., Abdulmalik, O., et al. (2018). Domain-focused CRISPR screen identifies HRI as a fetal hemoglobin regulator in human erythroid cells. Science 361, 285–290.

Hahn, C.K., and Lowrey, C.H. (2014). Induction of fetal hemoglobin through enhanced translation efficiency of γ-globin mRNA. Blood 124, 2730–2734.

Han, A.P., Fleming, M.D., and Chen, J.J. (2005). Heme-regulated eIF2α kinase modifies the phenotypic severity of murine models of erythropoietic protoporphyria and β-thalassemia. J. Clin. Invest.

Horlbeck, M.A., Gilbert, L.A., Villalta, J.E., Adamson, B., Pak, R.A., Chen, Y., Fields, A.P., Park, C.Y., Corn, J.E., Kampmann, M., and Weissman, J.S. (2016). Compact and highly active next-generation libraries for CRISPR-mediated gene repression and activation. eLife 5, e19760.

Huang, W., Sherman, B.T., and Lempicki, R.A. (2009). Systematic and integrative analysis of large gene lists using DAVID bioinformatics resources. Nat. Protoc. 4, 44–57.

Huang, P., Peslak, S.A., Lan, X., Khandros, E., Yano, J.A., Sharma, M., Keller, C.A., Giardine, B., Qin, K., Abdulmalik, O., et al. (2020). The HRI-regulated transcription factor ATF4 activates BCL11A transcription to silence fetal hemoglobin expression. Blood 135, 2121–2132.

Jacob, G.F., and Raper, A.B. (1958). Hereditary persistence of foetal haemoglobin production, and its interaction with the sickle-cell trait. Br. J. Haematol. 4, 138–149.

Jiang, J., Best, S., Menzel, S., Silver, N., Lai, M.I., Surdulescu, G.L., Spector, T.D., and Thein, S.L. (2006). cMYB is involved in the regulation of fetal hemoglobin production in adults. Blood 108, 1077–1083.

Kent, W.J., Sugnet, C.W., Furey, T.S., Roskin, K.M., Pringle, T.H., Zahler, A.M., and Haussler, D. (2002). The human genome browser at UCSC. Genome Res. 12, 996–1006.

Krämer, A., Green, J., Pollard, J., Jr., and Tugendreich, S. (2014). Causal analysis approaches in ingenuity pathway analysis. Bioinformatics 30, 523–530.

Kuleshov, M.V., Jones, M.R., Rouillard, A.D., Fernandez, N.F., Duan, Q., Wang, Z., Koplev, S., Jenkins, S.L., Jagodnik, K.M., Lachmann, A., et al. (2016). Enrichr: a comprehensive gene set enrichment analysis web server 2016 update. Nucleic Acids Res. 44 (W1), W90-7.

Kurita, R., Suda, N., Sudo, K., Miharada, K., Hiroyama, T., Miyoshi, H., Tani, K., and Nakamura, Y. (2013). Establishment of immortalized human erythroid progenitor cell lines able to produce enucleated red blood cells. PLoS ONE 8, e59890.

Landt, S.G., Marinov, G.K., Kundaje, A., Kheradpour, P., Pauli, F., Batzoglou, S., Bernstein, B.E., Bickel, P., Brown, J.B., Cayting, P., et al. (2012). ChIP-seq guidelines and practices of the ENCODE and modENCODE consortia. Genome Res. 22, 1813–1831.

Lechauve, C., Keith, J., Khandros, E., Fowler, S., Mayberry, K., Freiwan, A., Thom, C.S., Delbini, P., Romero, E.B., Zhang, J., et al. (2019). The autophagy-activating kinase ULK1 mediates clearance of free α-globin in β-thalassemia. Sci. Transl. Med. 11, eaav4881.

Lettre, G., Sankaran, V.G., Bezerra, M.A.C., Araújo, A.S., Uda, M., Sanna, S., Cao, A., Schlessinger, D., Costa, F.F., Hirschhorn, J.N., et al. (2008). DNA polymorphisms at the BCL11A, HBS1L-MYB, and β-globin loci associate with fetal hemoglobin levels and pain crises in sickle cell disease. Proc. Natl. Acad. Sci. U S A 105, 11869–11874.

Liang, J.R., Lingeman, E., Ahmed, S., and Corn, J.E. (2018). Atlastins remodel the endoplasmic reticulum for selective autophagy. J. Cell Biol. 217, 3354–3367.

Lingeman, E., Jeans, C., and Corn, J.E. (2017). Production of purified CasRNPs for efficacious genome editing. Curr. Protoc. Mol. Biol. 120, 1–19.

Liu, N., Hargreaves, V.V., Zhu, Q., Kurland, J.V., Hong, J., Kim, W., Sher, F., Macias-Trevino, C., Rogers, J.M., Kurita, R., et al. (2018). Direct promoter repression by BCL11A controls the fetal to adult hemoglobin switch. Cell 173, 430–442.e17.

Ma, Z., Zhu, P., Shi, H., Guo, L., Zhang, Q., Chen, Y., Chen, S., Zhang, Z., Peng, J., and Chen, J. (2019). PTC-bearing mRNA elicits a genetic compensation response via Upf3a and COMPASS components. Nature 568, 259–263.

Machanick, P., and Bailey, T.L. (2011). MEME-ChIP: motif analysis of large DNA datasets. Bioinformatics 27, 1696–1697.

Manca, L., and Masala, B. (2008). Disorders of the synthesis of human fetal hemoglobin. IUBMB Life 60, 94–111.

Magis, W., DeWitt, M.A., Wyman, S.K., Vu, J.T., Heo, S.-J., Shao, S.J., Henning, F., Romero, Z.G., Campo-Fernandez, B., McNeill, M., et al. (2019). High-level correction of the sickle mutation amplified in vivo during erythroid differentiation. bioRxiv. https://doi.org/10.1101/432716.

Masuoka, H.C., and Townes, T.M. (2002). Targeted disruption of the activating transcription factor 4 gene results in severe fetal anemia in mice. Blood 99, 736–745.

Meletis, J., Papavasiliou, S., Yataganas, X., Vavourakis, S., Konstantopoulos, K., Poziopoulos, C., Samarkos, M., Michali, E., Dalekou, M., Eliopoulos, G., et al. (1994). 'Fetal' erythropoiesis following bone marrow transplantation as estimated by the number of F cells in the peripheral blood. Bone Marrow Transplant. 14, 737–740.

Neph, S., Vierstra, J., Stergachis, A.B., Reynolds, A.P., Haugen, E., Vernot, B., Thurman, R.E., John, S., Sandstrom, R., Johnson, A.K., et al. (2012). An expansive human regulatory lexicon encoded in transcription factor footprints. Nature 489, 83–90.

Papayannopoulou, T., Vichinsky, E., and Stamatoyannopoulos, G. (1980). Fetal Hb production during Acute Erythroid Expansion: I. Observations in patients with transient erythroblastopenia and post-phlebotomy. Br. J. Haematol. 44, 535–546.

Park, S.H., Lee, C.M., Dever, D.P., Davis, T.H., Camarena, J., Srifa, W., Zhang, Y., Paikari, A., Chang, A.K., Porteus, M.H., et al. (2019). Highly efficient editing of the β-globin gene in patient-derived hematopoietic stem and progenitor cells to treat sickle cell disease. Nucleic Acids Res. 47, 7955–7972.

Pimentel, H., Bray, N.L., Puente, S., Melsted, P., and Pachter, L. (2017). Differential analysis of RNA-seq incorporating quantification uncertainty. Nat. Methods 14, 687–690.

Platt, O.S., Orkin, S.H., Dover, G., Beardsley, G.P., Miller, B., and Nathan, D.G. (1984). Hydroxyurea enhances fetal hemoglobin production in sickle cell anemia. J. Clin. Invest. 74, 652–656.

Robinson, J.T., Thorvaldsdóttir, H., Winckler, W., Guttman, M., Lander, E.S., Getz, G., and Mesirov, J.P. (2011). Integrative genomics viewer. Nat. Biotechnol. 29, 24–26.

Rochette, J., Craig, J.E., Thein, S.L., and Rochette, J. (1994). Fetal hemoglobin levels in adults. Blood Rev. 8, 213–224.

Rossi, A., Kontarakis, Z., Gerri, C., Nolte, H., Hölper, S., Krüger, M., and Stainier, D.Y.R. (2015). Genetic compensation induced by deleterious mutations but not gene knockdowns. Nature 524, 230–233.

Sankaran, V.G. (2011). Targeted therapeutic strategies for fetal hemoglobin induction. Hematology Am. Soc. Hematol. Educ. Program. 2011, 459–465.

Schiroli, G., Conti, A., Ferrari, S., della Volpe, L., Jacob, A., Albano, L., Beretta, S., Calabria, A., Vavassori, V., Gasparini, P., et al. (2019). Precise gene editing preserves hematopoietic stem cell function following transient p53-mediated DNA damage response. Cell Stem Cell 24, 551–565.e8.

Soler, E., Andrieu-Soler, C., de Boer, E., Bryne, J.C., Thongjuea, S., Stadhouders, R., Palstra, R.J., Stevens, M., Kockx, C., van Ijcken, W., et al. (2010). The genome-wide dynamics of the binding of Ldb1 complexes during erythroid differentiation. Genes Dev. 24, 277–289.

Stadhouders, R., Aktuna, S., Thongjuea, S., Aghajanirefah, A., Pourfarzad, F., Van IJcken, W., Lenhard, B., Rooks, H., Best, S., Menzel, S., et al. (2014). HBS1L-MYB intergenic variants modulate fetal hemoglobin via long-range MYB enhancers. J. Clin. Invest. 124, 1699–1710.

Steinmüller, L., and Thiel, G. (2003). Regulation of gene transcription by a constitutively active mutant of activating transcription factor 2 (ATF2). Biol. Chem. 384, 667–672.

Su, N., and Kilberg, M.S. (2008). C/EBP homology protein (CHOP) interacts with activating transcription factor 4 (ATF4) and negatively regulates the stress-dependent induction of the asparagine synthetase gene. J. Biol. Chem. 283, 35106–35117.

Suragani, R.N.V.S., Zachariah, R.S., Velazquez, J.G., Liu, S., Sun, C.W., Townes, T.M., and Chen, J.J. (2012). Heme-regulated eIF2α kinase activated Atf4 signaling pathway in oxidative stress and erythropoiesis. Blood 119, 5276–5284.

Thein, S.L., Menzel, S., Peng, X., Best, S., Jiang, J., Close, J., Silver, N., Gerovasilli, A., Ping, C., Yamaguchi, M., et al. (2007). Intergenic variants of HBS1L-MYB are responsible for a major quantitative trait locus on chromosome 6q23

influencing fetal hemoglobin levels in adults. Proc. Natl. Acad. Sci. U S A *104*, 11346–11351.

Vakulskas, C.A., Dever, D.P., Rettig, G.R., Turk, R., Jacobi, A.M., Collingwood, M.A., Bode, N.M., McNeill, M.S., Yan, S., Camarena, J., et al. (2018). A high-fidelity Cas9 mutant delivered as a ribonucleoprotein complex enables efficient gene editing in human hematopoietic stem and progenitor cells. Nat. Med. *24*, 1216–1224.

Wang, X., Angelis, N., and Thein, S.L. (2018). MYB: a regulatory factor in hematopoiesis. Gene *665*, 6–17.

Weinberg, R.S., Schofield, J.M., Lenes, A.L., Brochstein, J., and Alter, B.P. (1986). Adult 'fetal-like' erythropoiesis characterizes recovery from bone marrow transplantation. Br. J. Haematol. *63*, 415–424.

Wienert, B., Martyn, G.E., Kurita, R., Nakamura, Y., Quinlan, K.G.R., and Crossley, M. (2017). KLF1 drives the expression of fetal hemoglobin in British HPFH. Blood *130*, 803–807.

Wienert, B., Martyn, G.E., Funnell, A.P.W., Quinlan, K.G.R., and Crossley, M. (2018). Wake-up sleepy gene: reactivating fetal globin for β-Hemoglobinopathies. Trends Genet. *34*, 927–940.

Wienert, B., Wyman, S.K., Richardson, C.D., Yeh, C.D., Akcakaya, P., Porritt, M.J., Morlock, M., Vu, J.T., Kazane, K.R., Watry, H.L., et al. (2019). Unbiased detection of CRISPR off-targets in vivo using DISCOVER-Seq. Science *364*, 286–289.

Xiang, J., Wu, D.C., Chen, Y., and Paulson, R.F. (2015). In vitro culture of stress erythroid progenitors identifies distinct progenitor populations and analogous human progenitors. Blood *125*, 1803–1812.

Xu, J., Sankaran, V.G., Ni, M., Menne, T.F., Puram, R.V., Kim, W., and Orkin, S.H. (2010). Transcriptional silencing of γ-globin by BCL11A involves long-range interactions and cooperation with SOX6. Genes Dev. *24*, 783–798.

Xu, J., Shao, Z., Glass, K., Bauer, D.E., Pinello, L., Van Handel, B., Hou, S., Stamatoyannopoulos, J.A., Mikkola, H.K.A., Yuan, G.C., and Orkin, S.H. (2012). Combinatorial assembly of developmental stage-specific enhancers controls gene expression programs during human erythropoiesis. Dev. Cell *23*, 796–811.

Yu, G., Wang, L.G., and He, Q.Y. (2015). ChIP seeker: an R/Bioconductor package for ChIP peak annotation, comparison and visualization. Bioinformatics.

Zhang, Y., Liu, T., Meyer, C.A., Eeckhoute, J., Johnson, D.S., Bernstein, B.E., Nusbaum, C., Myers, R.M., Brown, M., Li, W., and Liu, X.S. (2008). Model-based analysis of ChIP-Seq (MACS). Genome Biol. *9*, R137.

Zhang, S., Macias-Garcia, A., Ulirsch, J.C., Velazquez, J., Butty, V.L., Levine, S.S., Sankaran, V.G., and Chen, J.J. (2019). HRI coordinates translation necessary for protein homeostasis and mitochondrial function in erythropoiesis. eLife *8*, e46976.

# STAR★METHODS

## KEY RESOURCES TABLE

| REAGENT or RESOURCE | SOURCE | IDENTIFIER |
|---|---|---|
| Antibodies | | |
| Human Fetal Hemoglobin APC | Thermo Fisher | Cat#: MHFH05; RRID:AB_1500105 |
| Anti-Human Fetal Hemoglobin FITC | BD Pharmigen | Cat#: 552829; RRID:AB_394480 |
| Anti-Hemoglobin B-(37-8) | Santa Cruz Biotechnology | Cat#: SC-21757; RRID:AB_627713 |
| rabbit anti-ATF4 | CST | Cat#: 11815S; RRID:AB_2616025 |
| mouse anti-BCL11A | Abcam | Cat#: ab19489; RRID:AB_2063996 |
| rabbit anti-LRF | ThermoFisher | Cat#: PA528144; RRID:AB_2545620 |
| mouse anti-GAPDH D4C6R | CST | Cat#: 97166S; RRID:AB_2756824 |
| Rabbit anti-GAPDH 14C10 | CST | Cat#: 2118S; RRID:AB_561053 |
| Rabbit anti-Fetal-Globin | Abcam | Cat#: ab137096; RRID:AB_2861154 |
| Rabbit anti-MYB D2R4Y | CST | Cat#: 12319S; RRID:AB_2716637 |
| donkey anti-mouse IRDye 680CW | Li-Cor | Cat#: 926-32222; RRID:AB_621844 |
| donkey anti-mouse IRDye 800CW | Li-Cor | Cat#: 926-32212; RRID:AB_621847 |
| donkey anti-rabbit IRDye 680CW | Li-Cor | Cat#: 926-32223; RRID:AB_621845 |
| donkey anti-rabbit IRDye 800CW | Li-Cor | Cat#: 926-32213; RRID:AB_621848 |
| rabbit IgG | Novus Biologicals | Cat#: NBP2-24891; RRID:AB_2811130 |
| Chemicals, Peptides, and Recombinant Proteins | | |
| Thapsigargin | Sigma | Cat#: T9033 |
| dexamethasone | Sigma | Cat#: D4902-100MG |
| doxycycline | Sigma | Cat#: D9891-1G |
| human stem cell factor | PeproTech | Cat#: 300-07 |
| erythropoietin | Peprotech | Cat#: 100-64 |
| heparin | Sigma | Cat#: H3149-25KU |
| insulin | Sigma | Cat#: I2643-25mg |
| erythropoietin | Peprotech | Cat#: 100-64 |
| holo-transferrin | Sigma | Cat#: T0665-100mg |
| mifepristone | Sigma | Cat#: M8046-100MG |
| Deposited Data | | |
| RNA-seq Data from HUDEP-2 Differentiation | NCBI-GEO | GEO: GSE153768 |
| ATF4 ChIP-seq from HUDEP-2 and primary erythroblasts | NCBI-GEO | GEO: GSE153768 |
| Experimental Models: Cell Lines | | |
| HUDEP-2 CRISPRi | This Study | N/A |
| HUDEP-2 HBBko | This Study | N/A |
| HUDEP-2 ATF4DN | This Study | N/A |
| HUDEP-2 ATF4ko-1/2 | This Study | N/A |
| K562 ATF4ko.562-1/2 | Gowen et al., 2015 | N/A |
| K562 ATF4ko.562-1/2 pFG12 Doxycycline-ATF4 | Gowen et al., 2015 | N/A |
| HUDEP-2 | | RRID:CVCL_VI06 |
| HUDEP-1 | | RRID:CVCL_VI05 |
| K562 | | RRID:CVCL_0004 |

*(Continued on next page)*

***Continued***

| REAGENT or RESOURCE | SOURCE | IDENTIFIER |
|---|---|---|
| Oligonucleotides | | |
| Protospacer sequences for all CRISPR KO or CRISPRi experiments | | See Table S2 |
| qPCR primer sequences | | See Table S3 |
| Primers for genotyping and knockout validation | | See Table S3 |
| Recombinant DNA | | |
| pEF1a-dCas9-HA-BFP-KRAB-NLS | Liang et al. (2018) | Addgene 102244 |
| Software and Algorithms | | |
| Li-Cor's ImageStudio software V5.2 | Li-Cor | https://www.licor.com/bio/image-studio/ |
| ImageJ | NIH | https://imagej.nih.gov/ij/ |
| Adobe Photoshop CS6 | Adobe | https://www.adobe.com/ |
| Adobe Illustrator CS6 | Adobe | https://www.adobe.com/ |
| FloJo 10 | BD | https://www.flowjo.com/ |
| Prism 6 | GraphPad | https://www.graphpad.com/scientific-software/prism/ |

## RESOURCE AVAILABILITY

### Lead Contact
Stable cell lines generated in this study are available from the Lead Contact, Jacob Corn (jacob.corn@biol.ethz.ch) with a complete Materials Transfer Agreement.

### Material Availability
This study did not generate new unique reagents.

### Data and Code Availability
The accession number for the RNA-seq data and the ChIP-seq data reported in this paper is deposited at NCBI-GEO: GSE153768.

## EXPERIMENTAL MODEL AND SUBJECT DETAILS

### Cell Lines
#### HUDEP-2 cell culture and differentiation
All cell culture was performed at 37°C in a humidified atmosphere containing 5% $CO_2$. HUDEP-2 cells were cultured in a base medium of SFEM (StemCell Technologies, Inc. 9650) containing to a final concentration of dexamethasone 1uM (Sigma D4902-100MG), doxycycline 1ug/ml (Sigma D9891-1G), human stem cell factor 50ng/ml (PeproTech 300-07), erythropoietin 50ng/ml (Peprotech 100-64), and penstrept 1%. Cells were cultured at a density of 2e5 – 1e6 cells/ml. For differentiation, HUDEP-2 cells are centrifuged at 500 g for 5 minutes, media is removed and replaced with differentiation media. Differentiation media consists of a base media of IMDM+Glutamax (ThermoFisher 31980030) containing to a final concentration human serum 5% (Sigma H4522-100mL), heparin 2IU/ml (Sigma H3149-25KU), insulin 10ug/ml (Sigma I2643-25mg), erythropoietin 50ng/ml (Peprotech 100-64), holo-transferrin 500ug/ml (Sigma T0665-100mg), mifepristone 1uM (Sigma M8046-100MG), and doxycyline 1ug/ml (Sigma D9891-1G). Cells are differentiated for 5 days and then harvested for analysis.

#### K562 cell culture
All cell culture was performed at 37°C in a humidified atmosphere containing 5% $CO_2$. K562 cells were grown in a base media of RPMI 1640 GlutaMAX (GIBCO 61870010) supplemented with 10% fetal bovine serum, 10% sodium pyruvate, and 1% penstrept. Cells were cultured at a density of 2e5 – 1e6 cells/ml. Stable expression of doxycycline-inducible ATF4 in K562 cells was generated as described previously (Gowen et al., 2015).

#### HEK293T cell culture
All cell culture was performed at 37°C in a humidified atmosphere containing 5% $CO_2$. HEK293T cells were grown in a base media of DMEM supplemented with 10% fetal bovine serum, 10% sodium pyruvate, and 1% penstrept. Cells were cultured at a density of 2e5 – 1e6 cells/ml.

## Primary Cell Cultures

### mPB-HSPCs cell culture and differentiation

All cell culture was performed at 37°C in a humidified atmosphere containing 5% CO2. For editing for human CD34+ cells, CD34+ mobilized peripheral blood HSPCs were thawed and cultured in SFEM containing CC110 supplement (StemCell Technologies, Inc. 02697) for 2 days. CD34+ cells were then electroporated and recovered for 24 hours in SFEM with CC110. After recovery, cells were transferred into erythroid expansion media containing SFEM and erythroid expansion supplement (StemCell Technologies, Inc. 02692) for 7 days and cultured at a density of 2e5-1e6 cells/ml. The resulting early erythroblasts were harvested for ChIP-seq or transferred to differentiation media containing SFEM with 50ng/ml erythropoietin, 3% normal human serum, and 1 μM mifepristone. The resulting late erythroblasts were harvested for analysis after 5 days of differentiation.

## METHOD DETAILS

### Generation of CRISPRi HUDEP-2 cells

WT-HUDEP-2 or *HBB* ko cells were transduced with lentivirus containing the construct EF1a-dCas9-HA-BFP-KRAB-NLS (Liang et al., 2018). The cells were FACs sorted for BFP expression and single-cell cloned. Individual clones were transduced with lentivirus containing guide RNAs targeting either *CD55, CD59, or HBB*. The clones were validated for successful knockdown by flow cytometry staining for extracellular markers CD55 and CD59 or intracellularly stained for β-globin.

### Lenti-viral Packaging

Lenti-viral packaging of all constructs was performed using HEK293T cells. TransIT®-LT1 Transfection Reagent (Mirus) was used following manufacturer's instructions. The plasmid mixture contained 50% construct plasmid, 40%DVPR, and 10% VSVG. Viral supernatant was harvested after 48 and 72 hours and filtered through 0.45 μM. For transduction of HUDEP-2 cells, cells were cultured in 50% HUDEP-2 media and 50% viral supernatant for 24 hours.

### sgRNA Plasmid Cloning

sgRNA guide sequences for CRISPRi transcriptional repression were obtained from the Weissman CRISPRi-v2 library (Horlbeck et al., 2016). The chosen guides were cloned into pGL1-library vector (Addgene 84832). All guides used are listed in Table S2.

### Cas9 RNP Nucleofection

Cas9 RNP was performed as described previously (Lingeman et al., 2017). Briefly, IVT guides are purified and complexed with purified Cas9-NLS protein. The nucleofection was performed using Lonza 4D-Nucleofector and using the P3 Primary Cell 96-well NucleofectorTM Kit (V4SP-3096) following manufacturer's instructions. The HUDEP-2 nucleofector code used was DD-100 and for primary HSPCs ER-100.

### IVT sgRNA

Guide RNAs were *in vitro* transcribed as described previously (Lingeman et al., 2017). Briefly, guide sequences were ordered as oligonucleotides and formed into duplexes using a PCR thermocycler. The DNA template was transcribed to RNA using HiScribe T7 High Yield RNA Synthesis Kit (E2040S) following manufacturer protocol. The resulting RNA was purified using RNeasy Mini kit (74104) and Rnase-Free DnaseI Kit (79254)

### High Pressure Liquid Chromatography and Mass Spectrometry

WT-HUDEP-2 and HBBko cells were differentiated and harvested for lysis in hemolysate reagent containing 0.005M EDTA and 0.07% KCN at 10,000 cells per microliter. The lysis was incubated at room temperature for ten minutes and then centrifuged at max speed for 5 minutes. The supernatant was collected and run on Agilent 1260 Infinity II using a PolyCAT A column, 35x4.6mm (3μm;1500Å) Serial# B19916E; Lot# 16-133-3 3.54CT0315. The following Buffer compositions were used: Mobile Phase A: 20mM Bis-tris, 2mM NaCN pH 6.8 and Mobile Phase B: 20mM Bis-tris, 2mM NaCN, 200mM NaCl, pH 6.9. The following flow settings were used: Gradient: 0-8' 2%–25% Phase B, 8-18' 25%–100% Phase B, 18-23' 100%–2% Mobile Phase B using a Flow Rate: 1.5mL/min and measuring detection of 415nm Diode Array. Three fractions from the HBBko and one fraction from the WT samples were collected and were then processed by the Proteomics group of Functional Genomics Center Zurich (FGCZ) for Proteolytic digestion ZipTip and analysis by LC/MS. Briefly, 100ul of samples were digested with trypsin (5 ng/ul in 10 mM Tris/2 mM CaCl2, pH 8.2) and 2 ul buffer (10 mM Tris/2 mM CaCl2, pH 8.2). Samples were microwaved for 30 minutes at 60C. The samples were dried, dissolved in 20 ul 0.1% TFA and subjected to C18 ZipTip desalting. The eluted sample (10ul of 50% CAN, 0.1%TFA) was dried, dissolved in 20ul of 0.1% FA and transferred to autosampler vials for LC/MS/MS and 1ul was used for injection.

### Intracellular FACs Staining

Staining was performed as adapted from the existing methods (Chung et al., 2019b). Briefly, undifferentiated or differentiated HUDEP-2 cells were centrifuged at 500 g for 5 minutes. The cells were washed with PBS with 0.1% BSA, re-centrifuged, and fixed in 0.05% glutaraldehyde. The fixed cells were centrifuged and washed and re-suspended in PBS with 0.1% BSA and 0.1% Triton

X-100 for permeabilization. The fixed and permeabilized cells were then centrifuged and washed. Antibodies were diluted in PBS with 0.1% BSA and incubated with cells for 20 minutes. The following antibody dilutions were used: Human Fetal Hemoglobin APC (Thermo Fisher MHFH05) 1:10, Anti-Human Fetal Hemoglobin FITC 1:10 (BD Pharmigen 552829), and Anti-Hemoglobin B-(37-8) PE/FITC 1:100 (Santa Cruz Biotechnology SC-21757 PE, SC-21757 FITC). After staining, the cells were centrifuged and washed twice before analysis by flow cytometry.

### RNA-Seq

WT-HUDEP-2 and HBBko cells were cultured and differentiated in triplicates. Cells were harvested and RNA was extracted using the RNeasy Mini kit 74104, Rnase-Free DnaseI Kit 79254 and Qiashredder 79654. RNA concentrations were quantified using Qubit RNA BR Assay (ThermoFisher) and 500ng were used for library preparation. RNA-seq library was made using Illumina TruSeq RNA Library Prep Kit v2 and following manufacturer's instructions. Paired-end 150bp reads were generated on a HiSeq4000. Reads for all eighteen samples (three replicates of HBBko and three WT HUDEP-2 samples at three time-points) were quantified using kallisto (Bray et al., 2016) and the hg38 index to assign reads to transcripts. Differential analysis of transcript abundance and consolidation of individual transcripts to gene-level abundance was calculated using sleuth (Pimentel et al., 2017).

### qRT-PCR

RNA was harvested from cells using QIAGEN RNeasy Mini Kit and Rnase-Free DnaseI Kit following manufacturer's instructions. RNA was reverse transcribed to cDNA using Iscript Reverse Transcription Supermix (BioRad) and qRT-PCR reactions were set up using SsoAdvanced Universal SYBR Green or SsoFast EvaGreen Supermix (BioRad). Reactions were run on the StepOne Plus Real-Time PCR System (Applied Biosystems) or the QuantStudio 6 Flex (Thermo Fisher). Samples were analyzed using a two-step amplification and melt curves were obtained after 40 cycles. The Ct values for genes of interest were normalized to GAPDH, and expressions of genes are represented as 2-[ΔCt] or 2-[ΔΔCt] for fold change over control condition. All primers used for qRT-PCR are listed in Table S2.

### ChIP-qPCR

ChIP was performed as described previously (Wienert et al., 2019). Briefly, 10 million cells per sample were harvested and cross-linked in 1% Formaldehyde. Cross-linking was quenched with the addition of 1.5M glycine. Samples were then lysed for 10 minutes at 4C in 50 mM HEPES–KOH, pH 7.5; 140 mM NaCl; 1 mM EDTA; 10% glycerol; 0.5% NP-40 or Igepal CA-630; 0.25% Triton X-100. Cells were then centrifuged at 1500 g for 3 minutes and the supernatant was discarded. The pellet was resuspended in 10 mM Tris–HCl, pH8.0; 200 mM NaCl; 1 mM EDTA; 0.5 mM EGTA and incubated for 5 minutes at 4C. The cells were then centrifuged at 1500 g for 3 minutes and the supernatant was discarded. The pellet was resuspended in 10 mM Tris–HCl, pH 8; 100 mM NaCl; 1 mM EDTA; 0.5 mM EGTA; 0.1% Na–Deoxycholate; 0.5% N-lauroylsarcosine and sonicated using the Covaris S220 following manufacturer's instructions. Protein A beads (ThermoFisher) were complexed with antibody and the antibody-bead complexes were incubated with cell lysates at 4C overnight with rotation. The antibodies used were rabbit anti-ATF4 (CST 11815S) and rabbit IgG (Novus Biologicals NBP2-24891). The beads were retrieved using a magnetic stand and rinsed with RIPA buffer. Elution buffer containing 50 mM Tris–HCl, pH 8; 10 mM EDTA; 1% SDS was added to the beads for reverse crosslinking at 65C overnight with shaking. After reverse crosslinking, the beads were removed. The eluted DNA was treated with RNaseA and Proteinase K and then purified using QIAGEN MinElute PCR Purification Kit, following the manufacturer's instructions. Q-PCR reactions were set up using SsoAdvanced Universal SYBR Green or SsoFast EvaGreen Supermix (BioRad). Reactions were run on the StepOne Plus Real-Time PCR System (Applied Biosystems) or the QuantStudio 6 Flex (Thermo Fisher). The Ct values were analyzed by the enrichment compared to input method.

### ChIP-seq

ChIP was performed as described in ChIP-qPCR method section. Sequencing library was prepared using NEBNext Ultra II DNA Library Prep Kit for Illumina (E7647) and NEBNext Multiplex Oligos for Illumina (Dual Index Primers Set 1) following manufacturer's instructions.

Paired-end 150bp reads were generated on an Illumina NextSeq500 at the Functional Genomics Center Zürich (FGCZ) and demultiplexed. FastQC (a quality control tool for high throughput sequence data. http://www.bioinformatics.babraham.ac.uk/projects/fastqc/) was used for initial quality control of reads. All samples, WT diff and undiff, HBBko diff and undiff, HSPC diff and undiff, ATF4-ΔN diff, ATF4KO3, and IgG and HSPC IgG diff and undiff, were processed according to ENCODE guidelines for unreplicated transcription factor ChIP-seq analysis

(Landt et al., 2012). In detail, raw reads were aligned against GRCh38 using bowtie2. Duplicate reads were marked using Picard's MarkDuplicates and multimapping, low quality, duplicated and non-properly paired reads were removed. Library complexity measures and flagstats were generated for each BAM file. BAM files were converted to tagAlign format and two subsampled pseudoreplicates were generated for each sample with half the total reads. Peak calling, fold change and p value signal tracks were generated using MACS2 (Zhang et al., 2008). Irreproducible Discovery Rate (IDR) analysis was performed using self-pseudoreplicates and the main samples to obtain self-consistent sets of peaks. Final peak calls were filtered by ENCODE blacklist (Amemiya et al., 2019) and an IDR of 2% and a signal value > 30.

Sets of peaks for each comparison were analyzed and associated to genes using the R package ChIPseeker (Yu et al., 2015) and Bioconductor hg38 TxDb (Team BC, Maintainer BP, 2019). TxDb.Hsapiens.UCSC.hg38.knownGene: Annotation package for TxDb object(s). R package version 3.4.6.). ChIP-seq peaks and RNA-seq results were merged using HGNC symbols using custom scripts. Figures were generated using the Integrative Genome Viewer (Robinson et al., 2011) and the UCSC Genome Brower (Kent et al., 2002). MEME-ChIP v5.1.1 (Machanick and Bailey, 2011) was used for motif discovery using peak boundaries +-250bp. FIMO v5.1.1 (Grant et al., 2011) was used to identify motif occurences for ATF4 (JASPAR matrix ID: MA0833.1) and GATA1 (JASPAR matrix ID: MA0035.4) with a p value less than 0.0001.

## Western Blot

Cells were harvested and lysed using RIPA buffer (Millipore) supplemented with Halt Protease Inhibitor Cocktail (ThermoFisher) and Phosphatase Inhibitor (ThermoFisher). Cell lysate concentrations were measured using Bradford reagent (VWR) or BCA assay (ThermoFisher). Cell lysates were normalized using NuPage LDS 4x Sample Buffer (Invitrogen) and samples were run on NU-PAGE Noves Bis-Tris 4%–12% gels (Invitrogen) in NuPAGE MES SDS Running Buffer at 180V for 40 minutes. Protein gels were transferred to a 0.4-$\mu$m nitrocellulose membranes at 1.3 A and 25 V for 15 to 20 minutes in a semi-dry apparatus (BioRad). After protein transfer, membranes were blocked in Tris-buffered saline with 1% Tween-20 (TBS-T) containing 5% nonfat milk for 30 minutes at room temperature with rocking. Primary antibodies were diluted in TBST containing 5%BSA and 0.1% sodium azide. The following antibody concentrations were used: rabbit anti-ATF4 (CST 11815S) 1:1000, mouse anti-BCL11A (Abcam ab19489) 1:1000, rabbit anti-LRF (ThermoFisher PA528144) 1:1000, mouse anti-GAPDH D4C6R (CST 97166S) 1:1000, Rabbit anti-GAPDH 14C10 (CST 2118S) 1:1000, Mouse anti-B-Globin (SCBT sc-21757) 1:500, Rabbit anti-Fetal-Globin (Abcam ab137096) 1:1000, Rabbit anti-MYB D2R4Y (CST 12319S) 1:1000. Membranes were rinsed in TBST and incubated with antibody for 2 hours at room temperature or 4C overnight with rocking. After incubation, membranes are rinsed twice with TBST for 5 minutes. Secondary antibodies are diluted in 1% Tween-20 (TBS-T) containing 5% nonfat milk and incubated at room temperature for 30 minutes with rocking. The secondary antibodies used for western blotting were obtained from Li-Cor and are as follows: donkey anti-mouse IRDye 680CW (926-32222), donkey anti-mouse IRDye 800CW (926-32212), donkey anti-rabbit IRDye 680CW (926-32223), and donkey anti-rabbit IRDye 800CW (926-32213). Membranes are then rinsed twice with TBST for 5 minutes each. Membranes are rinsed with PBS for 5 minutes and then imaged using Li-Cor Odyssey CLx.

## QUANTIFICATION AND STATISTICAL ANALYSIS

All analysis was performed using data from at least three independent biological replicates (exact number of replicates are stated in the figure legend). All statistical analyses were performed in PRISM6 software using paired Student's t test. P values are indicated as follow: * < 0.05, ** < 0.01, *** < 0.001, **** < 0.0001. The distribution of the data was assumed to be normal, but this was not formally tested.

**Supplemental Information**

**ATF4 Regulates MYB to Increase γ-Globin**

**in Response to Loss of β-Globin**

Mandy Y. Boontanrart, Markus S. Schröder, Gautier M. Stehli, Marija Banović, Stacia K. Wyman, Rachel J. Lew, Matteo Bordi, Benjamin G. Gowen, Mark A. DeWitt, and Jacob E. Corn
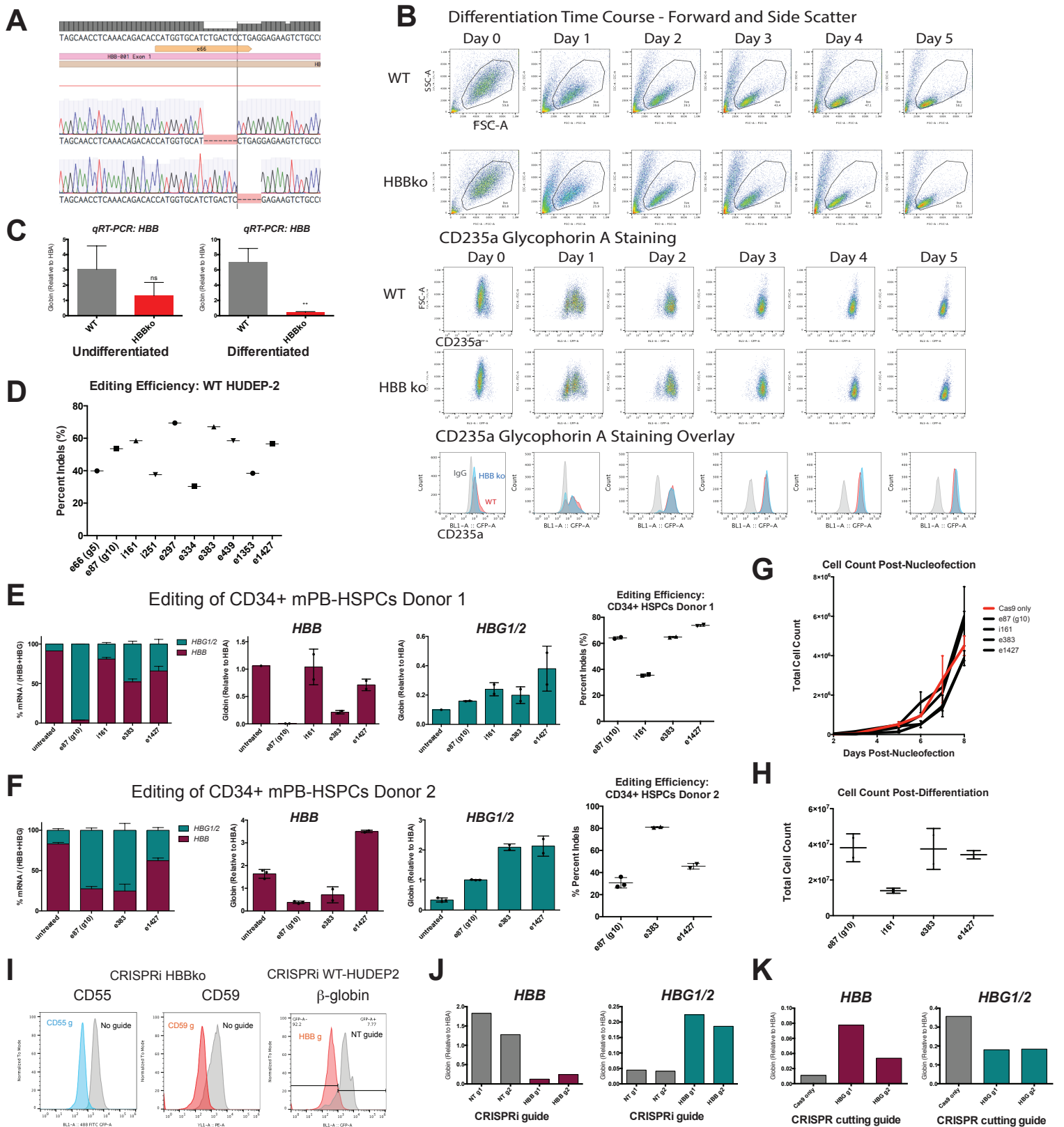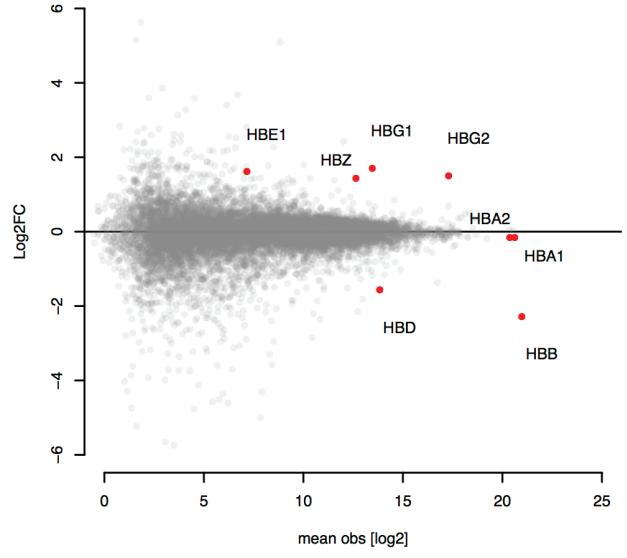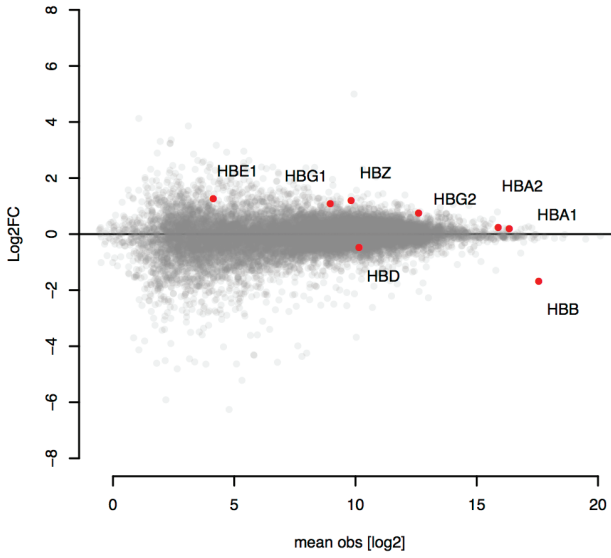
**Supplement Figure 1 (related to Figure 1)**

A) Schematic showing the e66 (g5) guide location in HBB, with the cut site indicated by a black line. The HBBko clone was genotyped by TA cloning of the HBB locus followed by Sanger sequencing. Two alleles were found: a 5- and 7-basepair deletion. B) Flow cytometry plots showing forward and side scattering of WT and HBBko over the course of 5 days in differentiation media. Cells were stained for CD235a (Glycophorin A) and shown as dot plots and overlaid histograms to compare WT to HBBko during differentiation in red and blue, respectively. IgG isotype control trace is in gray. C) qRT-PCR of HBB in undifferentiated and differentiated cells comparing transcript expression levels between WT and HBBko cells. P value indicates paired, two-tailed student t test (ns, non-significant; *, P ≤ 0.005). D) Editing efficiency of the panel of HBB guides in HUDEP-2 cells as measured by TIDE analysis. E) Mobilized peripheral blood CD34+ cells from a healthy donor were edited with a subset of the HBB guides, recovered in erythroid expansion media, differentiated for 5 days, and analyzed for qRT-PCR for HBB and HBG 1/2 for (n=2) technical replicates for one healthy donor. Editing efficiency was measured by TIDE. F) Data from healthy donor 2. G)Total cell counts of edited CD34+ cells during recovery in erythroid expansion media. Data is shown as the mean ± SEM of (n=2) technical replicates for one healthy donor. H) Total cell counts of edited CD34+ cells after 5 days of differentiation. Data is shown as the mean ± SD of (n=2) technical replicates for one healthy donor. I) HBBko CRISPRi cell line was validated using guides targeting CD55 and CD59. FACs staining was used for validating knockdown of the cell marker. WT-CRISPRi cell line was validated using an HBB guide and differentiated and intracellularly stained for B-globin protein and compared to non-targeting guide. J) qRT-PCR of HBB and HBG1/2 for CRISPRi knockdown of HBB in WT differentiated cells. Data is shown for one replicate. K) qRT-PCR of HBB and HBG1/2 from pooled knockout of HBG1/2 in HUDEP-1 cells. N=2 technical replicates are shown as mean.
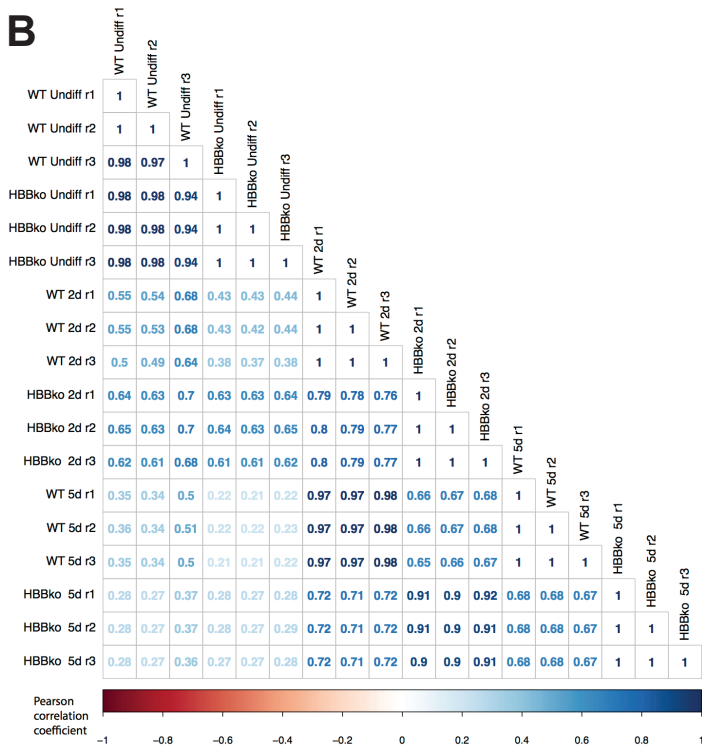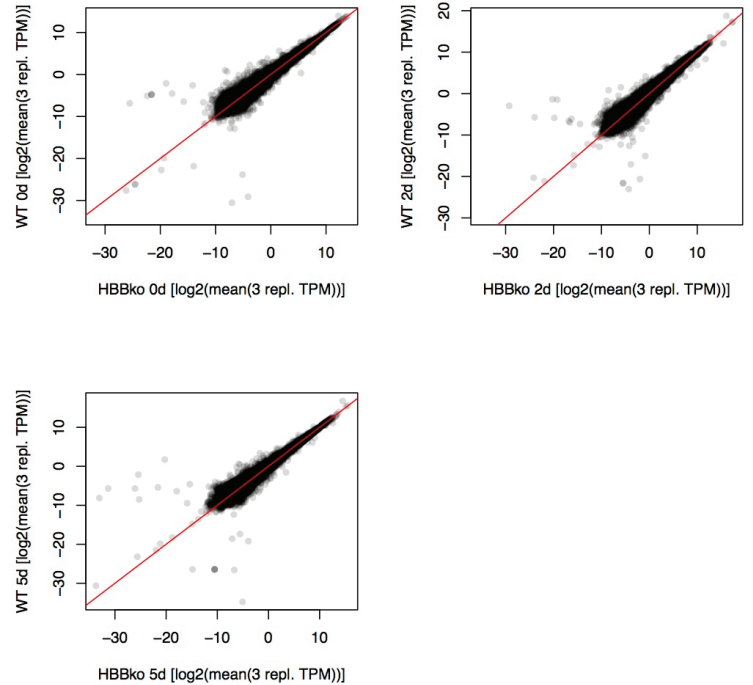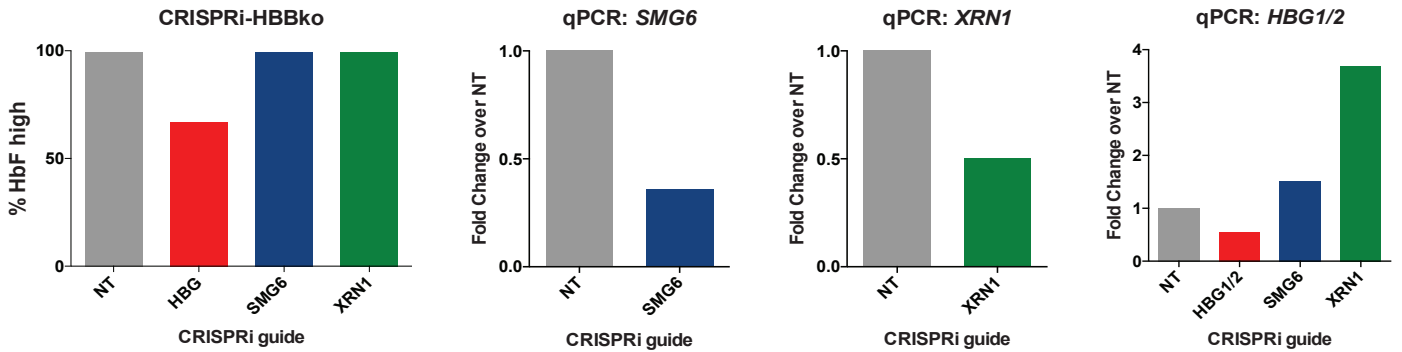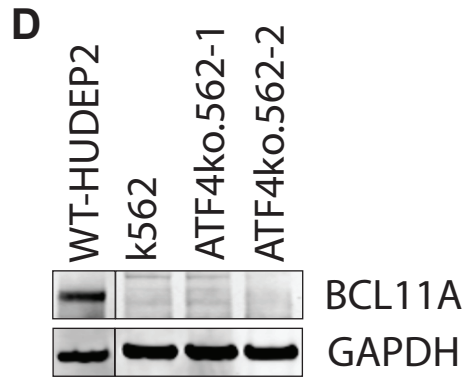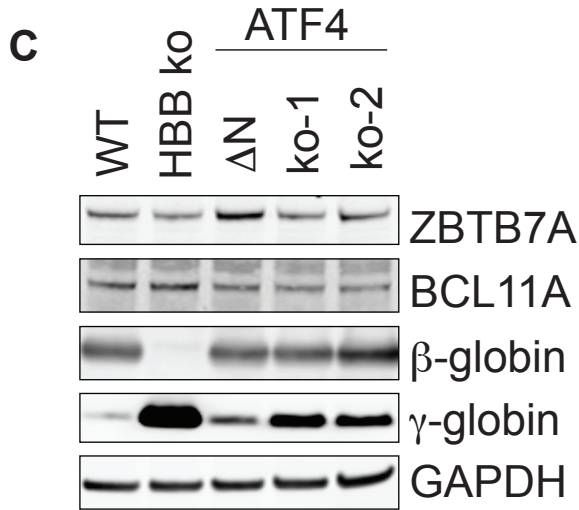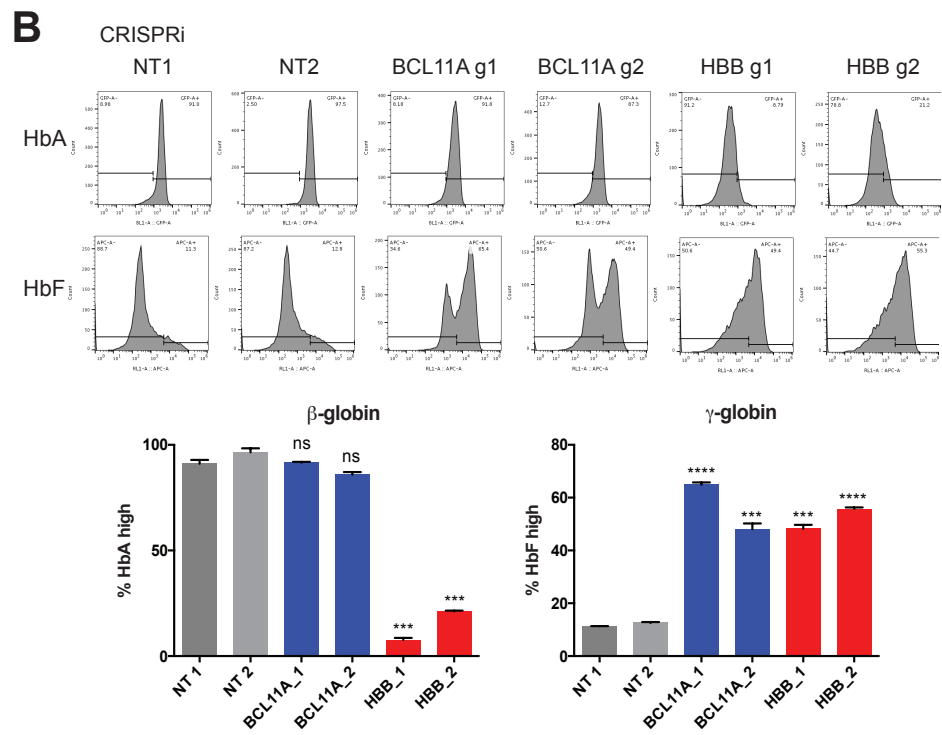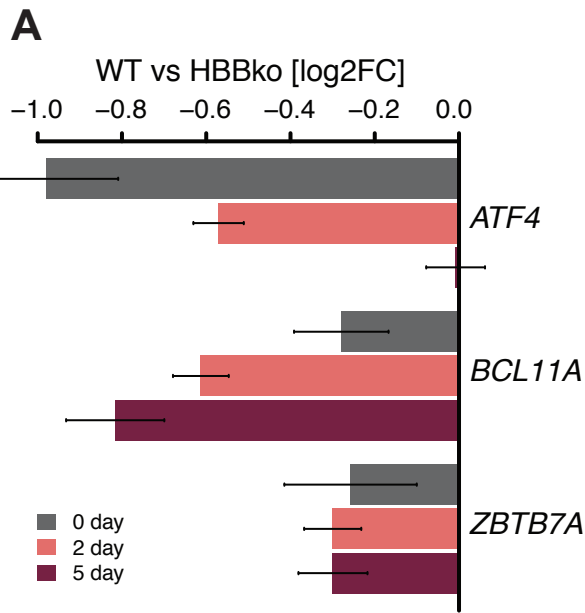
**Supplement Figure 2 (related to Figure 2)**

A) MA plots of RNAseq data for undifferentiated cells and 2 day differentiation, with globin genes highlighted.

B) Pearson correlation matrix of RNAseq samples, highlighting inter-condition reproducibility and differences between conditions.

C) Pearson correlation analysis of RNAseq data comparing WT to HBBko at three different time points of differentiation

D) Leftmost panel shows quantified intracellular flow staining of γ-globin for HBBko CRISPRi cells expressing either non-targeting, HBG1/2, SMG6, or XRN1 guide. Right three panels show qRT-PCR for SMG6, XRN1, or HBG1/2 for knockdown validation.
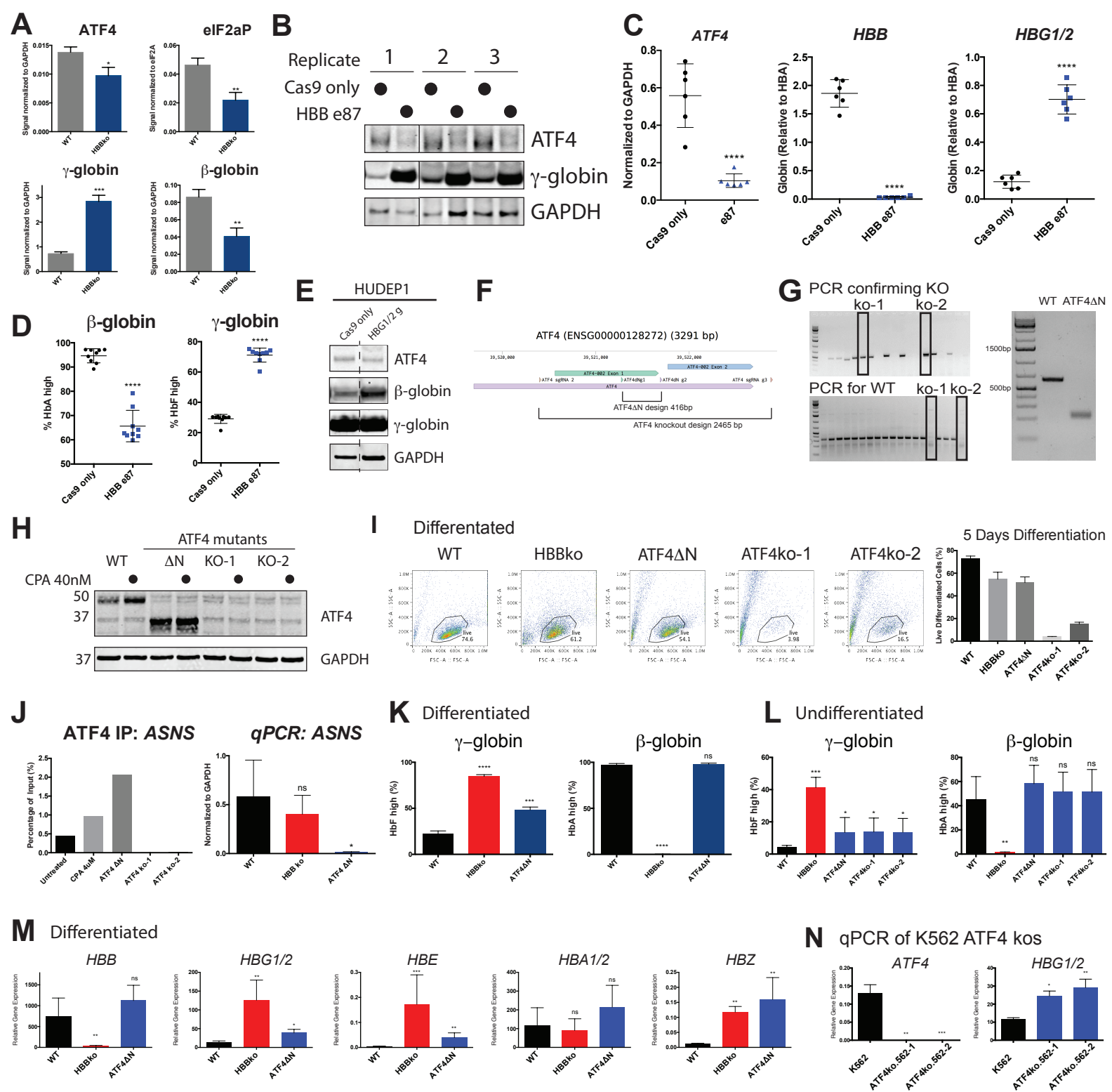
**Supplement Figure 3 (related to Figure 3)**

A) Quantification of western blot from Fig 3A. The data is shown as the mean ± SD of 3 biological replicates. P value indicates paired, two-tailed student t test (*, P ≤ 0.05; **, P ≤ 0.005; ***, P ≤ 0.001). B) HUDEP-2 cells were pool-edited with HBB guide e87 (g10) and differentiated for 5 days. Western blot shows ATF4 and γ-globin. The image shows 3 biological replicates and is from the same blot with the solid line indicating irrelevant conditions removed. C) qRT-PCR of ATF4, HBB, and HBG1/2 from HBB pooled editing and 5 day differentiated HUDEP-2 cells from A). Data is shown as six biological replicates. P value indicates unpaired, two-tailed student t test (****, P ≤ 0.0001). D) Intracellular Flow cytometry staining for HbA and HbF from pooled editing and 5 day differentiated HUDEP-2 cells from A). P value indicates unpaired, two-tailed student t test (****, P ≤ 0.0001). Data is shown as six biological replicates. E) HUDEP-1 cells were edited with guide targeting HBG1/2 and differentiated for 5 days. Western blot shows ATF4, β-globin, and γ-globin. The image is from the same blot with the dotted line indicating irrelevant conditions removed. F) Schematic of ATF4 with sgRNAs used for generation of ATF4 knockouts and ATF4ΔN. See Table S2 for all guide sequences. G) PCR genotyping of ATF4ko-1 and ATF4ko-2 clones. Top panel shows PCR amplification using primers outside the cut region. Successful ATF4 deletion is indicated by ~500 base pair fragment. Unsuccessful deletion results in failure of PCR amplification due to the large size. Lower panel shows PCR amplification of a region within the ATF4 gene. Successful deletion of ATF4 is indicated by no amplification. Right panel: PCR genotyping of ATF4ΔN using primers flanking the ATF4ΔN cut sites. TA-cloning and Sanger sequencing revealed one 398- and one 415-basepair deletion for the ATF4ΔN clone. H) Western blotting for ATF4 of WT and ATF4 mutant clones treated with 40nM cyclopiazonic acid (CPA) for 16 hours. ATF4ΔN removes the amino terminal regulatory region but retains the C-terminal DNA binding domain. I) Flow cytometry plots of forward and side scatter 5 days post differentiation of WT, HBBko, ATF4ΔN, ATF4ko-1, and ATF4ko-2. Right panel shows percentages of differentiated cells as the mean ± SD of 3 biological replicates. J) ATF4 CHIP-qPCR for the ASNS promoter region shows ATF4 binding at WT and ATF4ΔN and loss of binding for ATF4ko-1 and ATF4ko-2 in undifferentiated cells. The data is shown as one replicate. Right panel shows qRT-PCR on differentiated cells for ASNS. The data is shown as the mean ± SD of 3 biological replicates. P value indicates paired, two-tailed student t test (ns, non-significant; *, P ≤ 0.05). K) Quantification of intracellular FACs staining of differentiated WT, HBBko, and ATF4ΔN cells. Data is presented as mean ± SD of 3 biological replicates. P value indicates paired, two-tailed student t test (ns, non-significant; ***, P ≤ 0.001; ****, P ≤ 0.0001). L) Quantification of intracellular FACs staining of undifferentiated WT, HBBko, ATF4ΔN, and ATF4ko cells. Data is presented as mean ± SD of 4 biological replicates. P value indicates paired, two-tailed student t test (ns, non-significant; *, P ≤ 0.05; **, P ≤ 0.005). M) qRT-PCR of globin gene expression relative to GAPDH for differentiated WT, HBBko, and ATF4ΔN. Data is presented as mean ± SD of 3 biological replicates. P value indicates paired, two-tailed student t test (ns, non-significant; *, P ≤ 0.05; **, P ≤ 0.005; ***, P ≤ 0.001) N) qRT-PCR of ATF4 and HBG1/2 relative to GAPDH in K562 WT cells and two K562 ATF4 knockout clones. Data is presented as mean ± SD of 3 biological replicates. P value indicates paired, two-tailed student t test (*, P ≤ 0.05; **, P ≤ 0.005; ***, P ≤ 0.001).
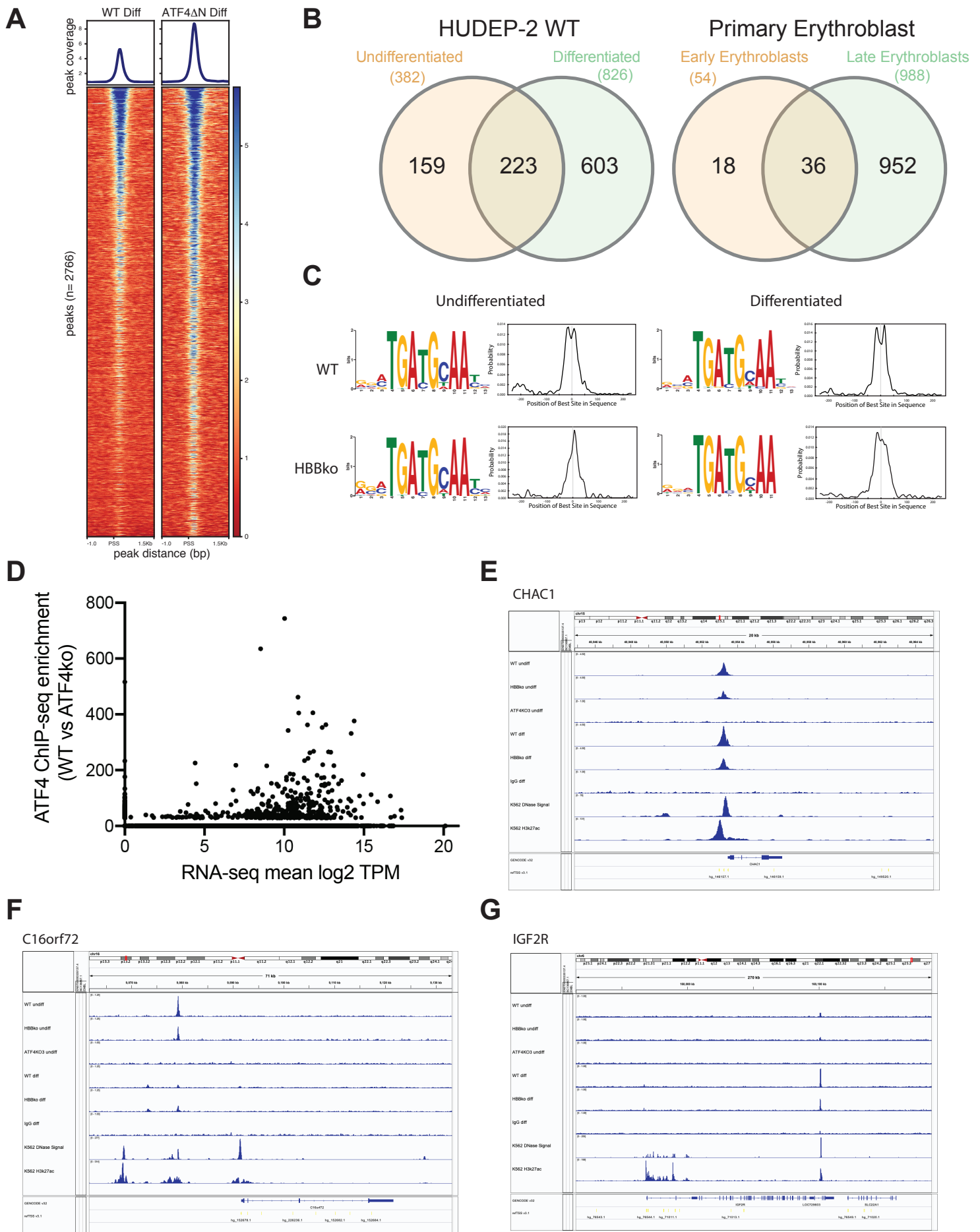
**Supplement Figure 4 (related to Figure 4 and 5)**
A) ATF4, BCL11A, and ZBTB7A transcript levels in HBBko HUDEP-2 cells are shown as log2 fold change relative to WT cells undifferentiated, after 2 days of differentiation, and after 5 days of differentiation.
B) Top panel shows intracellular FACs staining of differentiated cells for HbA and HbF in WT CRISPRi cells with guides against non-targeting, BCL11A, and HBB. Lower panel shows quantified data as mean ± SD of 3 biological replicates. P value indicates paired, two-tailed student t test (ns, non-significant; ***, P ≤ 0.001; ****, P ≤ 0.0001).
C) Western blot of undifferentiated WT, HBBko, ATF4ΔN, and ATF4ko cells.
D) Western blot of K562 WT, ATF4ko.562-1 and ATF4ko.562-2 for BCL11A expression. Image is from the same blot with the black line indicating irrelevant conditions removed.

**Supplement Figure 5 (related to Figure 5)**

A) Heatmap showing ATF4 ChIP-seq fold change over control for all peaks across samples. ChIP-seq samples shown are differentiated WT and ATF4DN. B) Venn diagrams showing overlap of high confidence ATF4 peaks between WT undifferentiated and differentiated (left) and between primary early erythroblasts and late erythroblasts (right). C) Unbiased motif discovery (MEME) for ChIP-seq samples WT and HBBko undifferentiated and differentiated for identification of the consensus sequence. D) ATF4 ChIP-seq signal enrichment in WT HUDEP-2 cells and corresponding RNA-seq log2 TPM values. E) CHAC1 raw read coverage for ATF4 ChIP-seq. Tracks show library size normalized tags per million (TPM) coverage of WT undiff and diff, HBBko undiff and diff, ATF4KO3 undiff and IgG data. DNase signal and H3k27ac tracks show reference ENCODE data from K562 cells. Annotation tracks show GENCODE v32 gene annotation and transcription start site annotation from refTSS v3.1 F) C16orf72 raw read coverage for ATF4 ChIP-seq. G) IGF2R1 raw read coverage for ATF4 ChIP-seq.
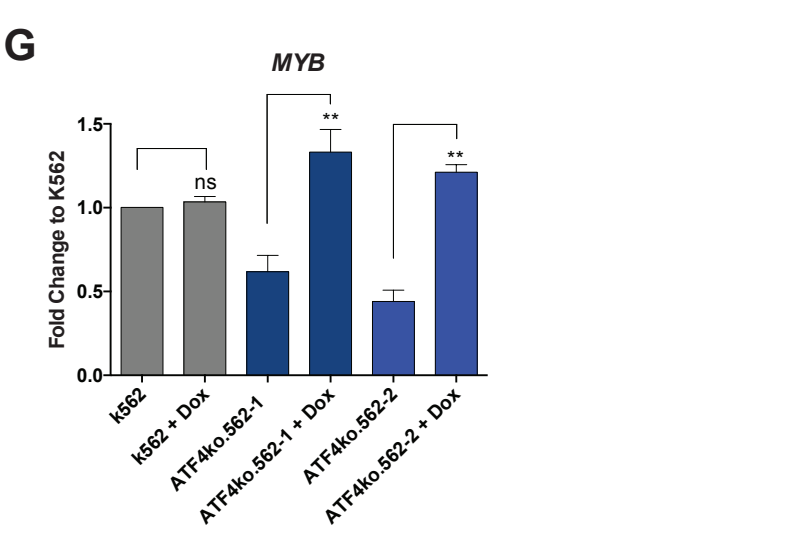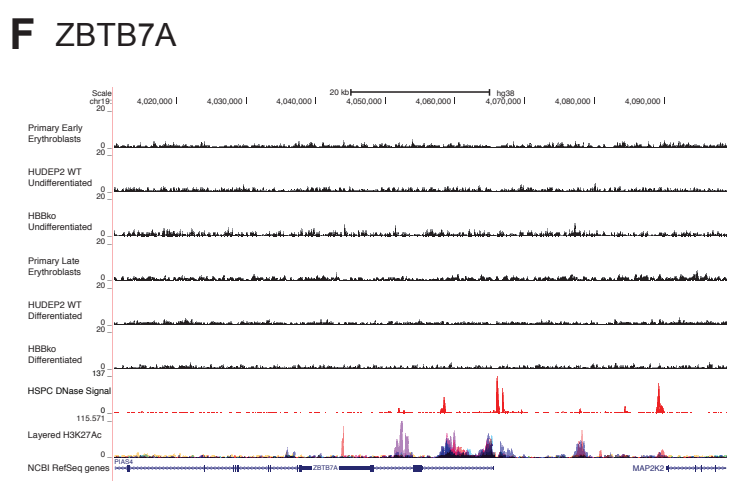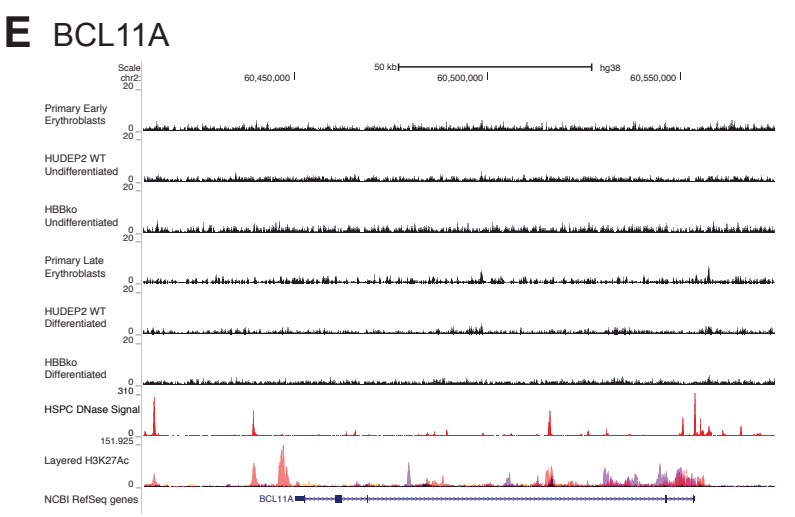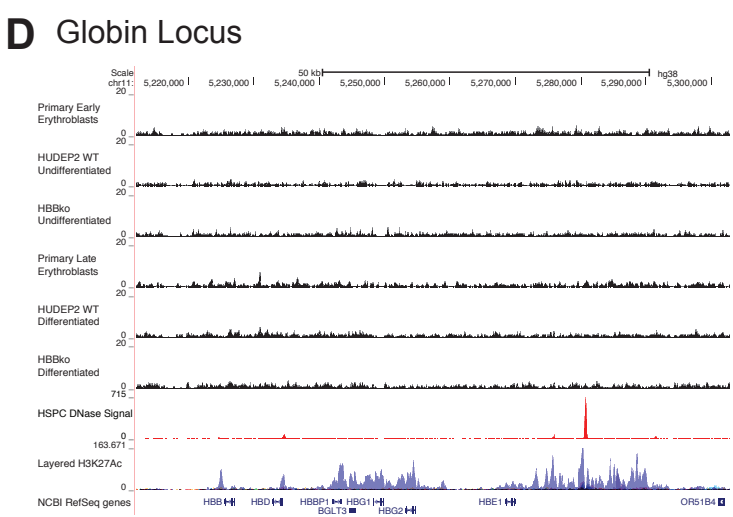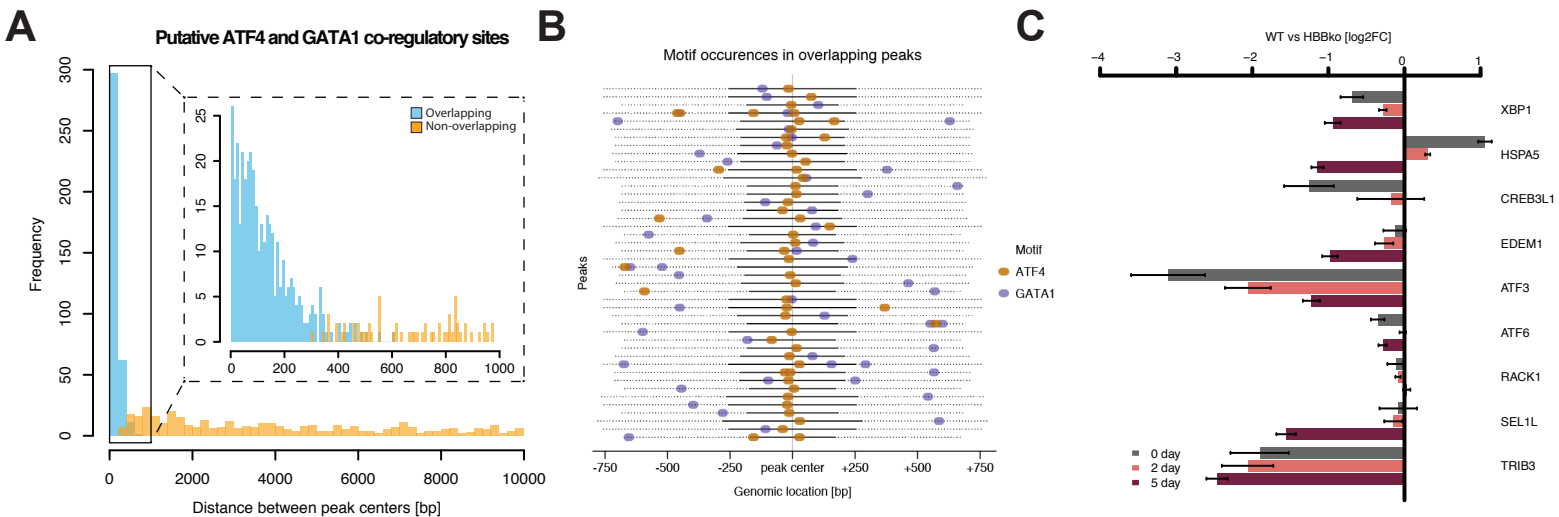
**Supplement Figure 6 (related to Figure 5 and 6)**

A) Distances between ATF4 and GATA1 peaks annotated as binding at the same gene. ATF4 peaks with a GATA1 peak within 10kb (n=753, outer panel) or within 1kb (n=434, inner panel) between peak centers are shown. Distances for overlapping ATF4 and GATA1 peaks are shown in blue (n=371), non-overlapping peaks that are still adjacent to the same gene are shown in orange (n=382).

B) Motif occurrences in overlapping ATF4 and GATA1 peaks. Centered ATF4 peak regions are shown (black solid lines) with 500bp extensions on both sides (dotted lines) for 44 ATF4 peaks that overlapped with GATA1 peaks. FIMO v5.1.1 was used to identify motif occurrences for ATF4 (JASPAR matrix ID: MA0833.1) and GATA1 (JASPAR matrix ID: MA0035.4) with a p-value less than 0.0001. ATF4 motif occurrences are shown in brown, GATA1 motif occurrences in blue.

C) Transcript levels of UPR targets in HBBko HUDEP-2 cells are shown as log2 fold change relative to WT cells undifferentiated, after 2 days of differentiation, and after 5 days of differentiation.

D) ATF4 ChIP-seq enrichment tracks for the globin locus. DNAse signal is from previously published primary human CD34+ cells (Neph et al., 2012). H3k27ac tracks show reference ENCODE data from K562 cells.

E) ATF4 ChIP-seq fold enrichment tracks for the BCL11A locus.

F) ATF4 ChIP-seq fold enrichment tracks for the ZBTB7A locus.

G) qRT-PCR for MYB expression in K562 and ATF4ko.562-1/2 with doxycycline-inducible ATF4 constructs treated with 100ng/ml doxycycline for 48 hours. The data is presented as mean ± SD of three biological replicates. P value indicates unpaired, two-tailed student t test (ns, non-significant; **, P 0.005).

**Table S1: Mass Spectrometry Spectrum Counts from HPLC elutions, Related to Figure 1.**
Peaks 1, 2, and 3 are elutions from differentiated HBBko cells at 5 minutes, 7 minutes, and 7.5 minutes, respectively. Peak 4 is the elution from differentiated WT cells at 10 minutes.

| Alternate ID | Molecular Weight | Peak 1 | Peak 2 | Peak 3 | Peak 4 |
|---|---|---|---|---|---|
| HBA1 | 15 kDa | 31 | 88 | 108 | 224 |
| HBB | 16 kDa | 8 | 15 | 20 | 278 |
| HBB | 16 kDa | 4 | 7 | 6 | 186 |
| HBD | 16 kDa | 2 | 4 | 7 | 7 |
| HBG2 | 16 kDa | 43 | 146 | 79 | 10 |
| HBG2 | 16 kDa | 9 | 30 | 14 | 2 |
| HBG1 | 16 kDa | 8 | 18 | 10 | 1 |
| GPI | 63 kDa | 0 | 0 | 12 | 39 |
| GOT2 | 48 kDa | 0 | 10 | 23 | 2 |
| TUBA1A | 50 kDa | 13 | 10 | 6 | 3 |
| RACK1 | 35 kDa | 3 | 2 | 14 | 12 |
| ENO1 | 47 kDa | 0 | 5 | 9 | 17 |
| ENO1 | 47 kDa | 0 | 4 | 7 | 15 |
| ENO2 | 47 kDa | 0 | 0 | 0 | 1 |
| GMPS | 77 kDa | 0 | 16 | 12 | 0 |
| PPIA | 18 kDa | 14 | 12 | 2 | 0 |
| CA2 | 29 kDa | 13 | 5 | 4 | 5 |
| PEBP1 | 21 kDa | 19 | 5 | 3 | 0 |
| FSCN1 | 55 kDa | 0 | 2 | 12 | 12 |
| RPL7 | 29 kDa | 9 | 10 | 3 | 2 |
| TUBB | 50 kDa | 8 | 7 | 5 | 4 |
| TUBB | 50 kDa | 2 | 2 | 1 | 1 |
| TUBB4B | 50 kDa | 1 | 1 | 1 | 0 |
| EEF1A1 | 50 kDa | 9 | 6 | 6 | 2 |
| HSPA8 | 71 kDa | 7 | 6 | 6 | 3 |
| PSMA7 | 28 kDa | 4 | 7 | 4 | 7 |
| MDH1 | 36 kDa | 13 | 6 | 2 | 0 |
| CFL1 | 19 kDa | 9 | 4 | 5 | 2 |
| FH | 55 kDa | 7 | 10 | 2 | 0 |
| RPL6 | 33 kDa | 10 | 7 | 2 | 0 |
| UROD | 41 kDa | 0 | 5 | 13 | 0 |
| HIST1H4A | 11 kDa | 6 | 7 | 3 | 2 |
| GARS | 83 kDa | 0 | 2 | 0 | 15 |
| TKT | 68 kDa | 0 | 0 | 0 | 17 |

**Table S2: CRISPR/Cas9 and CRISPRi sgRNA sequences used in this study, Related to STAR methods sections on sgRNA Plasmid Cloning and IVT sgRNA.**

| Construct | Protospacer | Source |
|---|---|---|
| pLG1-puro HBB g1 sgRNA | TAGACCACCAGCAGCCTAA | Horlbeck et al. 2016 |
| pLG1-puro HBB g2 sgRNA | GAACTTCAGGGTGAGTCTA | Horlbeck et al. 2016 |
| pLG1-puro Non-targeting 1 sgRNA | CGCCAAACGTGCCCTGACGG | Horlbeck et al. 2016 |
| pLG1-puro Non-targeting 2 sgRNA | GCTCGGTCCCGCGTCGTCG | Horlbeck et al. 2016 |
| pLG1-puro BCL11A g1 sgRNA | GCTTGCGGCGAGACATGGT | Horlbeck et al. 2016 |
| pLG1-puro BCL11A g2 sgRNA | GAGAGCCGGGTTAGAAAGA | Horlbeck et al. 2016 |
| pLG1-puro SMG6 sgRNA | ctcctccccgctcggccct | Horlbeck et al. 2016 |
| pLG1-puro XRN1 sgRNA | CTCGAAAGCCCCAGCTCTA | Horlbeck et al. 2016 |
| pLG1-puro CD55 sgRNA | GCTGCGACTCGGCGGAGTCC | Horlbeck et al. 2016 |
| pLG1-puro CD59 sgRNA | GCGCAGAAGCGGCTCGAGGC | Horlbeck et al. 2016 |
| e66 (g5) | CATGGTGCATCTGACTCCTG | DeWitt et al. 2016 |
| e87 (g10) | CTTGCCCCACAGGGCAGTAA | DeWitt et al. 2016 |
| i161 | TGGTATCAAGGTTACAAGAC | This Study |
| i251 | GGGTGGGAAAATAGACCAAT | This Study |
| e297 | TGGTCTACCCTTGGACCCAG | This Study |
| e334 | GCCCATAACAGCATCAGGAG | This Study |
| e383 | GCTCATGGCAAGAAAGTGCT | This Study |
| e439 | CAGCTCACTCAGTGTGGCAA | This Study |
| e1353 | CACAGACCAGCACGTTGCCC | This Study |
| e1427 | GCAGGCTGCCTATCAGAAAG | This Study |
| ATF4dN g1 | AGTCCCGCCTCATAAGTGGA | This Study |
| ATF4dN g2 | ATCCCACCAGGACGATG | This Study |
| ATF4 sgRNA 2 | CTCGTCACAGCTACGCCCT | Gowen et al. 2016 |
| ATF4 sgRNA 3 | TGGCCAACTATACGGCTCCA | Gowen et al. 2016 |

**Table S3: Primers for qRT-PCR, ChIP-qPCR, and amplification for genotyping and knockout validations, Related to Star Methods sections on qRT-PCR, ChIP-qPCR, and Cas9 RNP Nucleofection.**

**Primers for qRT-PCR**

| Target | Forward | Reverse |
|---|---|---|
| HBB | TGTCCACTCCTGATGCTGTTATG | GGCACCGAGCACTTTCTTG |
| HBG1/2 | CCTGTCCTCTGCCTCTGCC | GGATTGCCAAAACGGTCAC |
| HBA | GGGTGGACCCGGTCAACTT | GAGGTGGGCGGCCAGGGT |
| HBE | TGCTGAGGAGAAGGCTGCCG | TGGGTCCAGGGGTAAACAACGAGG |
| HBZ | GAGGACCATCATTGTGTCCA | AGTGCGGGAAGTAGGTCTTG |
| GAPDH | CAACAGCGACACCCACTCCT | CACCCTGTTGCTGTAGCCAAA |
| SMG6 | GCACGCATGGTGAACAGAAA | TGTTCAGCTCTCATTCTCGTCC |
| XRN1 | TGGCTTACTGGTACATGGGC | TCATGCCTAAGGAGCCCAAC |
| ASNS | ACTGGCTGCTAGAAAGGTGG | GCCTGAATGCCTTCCTCAGA |
| MYB | CGCAGCCATTCAGAGACACT | GCTGCATGTGTGGTTCTGTG |

**Primers for ChIP-qPCR**

| | Forward | Reverse |
|---|---|---|
| ASNS promoter | ATGATGAAACTTCCCGCACG | GGGATGTGGACAGCTTGACG |

**Primers for knockout validation and genotyping**

| | Forward | Reverse |
|---|---|---|
| ATF4 WT for | CATTCCTCGATTCCAGCAAAGC | TGAGTGATGGGGCCAAGTGAG |
| ATF4 knockout for | CGTCCTCGGCCTTCACAATA | TCTTCAGGATGAGGCTTCTGC |
| ATF4DN | CCT GGT CTC CGT GAG CGT C | CATCCAATCTGTCCCGGAGAAGG |
| HBB exon 1-2 | ATG CTT AGA ACC GAG GTA GAG TTT | CCT GAG ACT TCC ACA CTG ATG |
| HBB exon 3 | AGGCAGAATCCAGATGCTCAAGGC | GCA CGT GGA TCC TGA GAA CTT CAG |